Malaysian Journal of Chemistry, 2026, Vol. 28(2), 80-109

Phytochemical Profiling and Bioactivities of *Myristica fragrans* Leaf Fractions via GC-MS, LC-HRMS, and Molecular Docking

Ariyanti Saputri[1,2], Sofa Fajriah[1]*, Antonius Herry Cahyana[2,]*, Ziyan Saputra[1,2] and Marissa Angelina[1]

[1]Research Center for Pharmaceutical Ingredients and Traditional Medicine, National Research and Innovation Agency Republic of Indonesia, Cibinong, West Java, Indonesia

[2]Chemistry Department, University of Indonesia, Depok, West Java, Indonesia

*Corresponding author (e-mail: sofa001@brin.go.id)

This study integrates GC-MS/LC-HRMS profiling with antioxidant and antiproliferative assays to map fraction-resolved chemistry of *Myristica fragrans* leaves. Phytochemical screening indicated non-polar metabolites in the hexane fraction and phenolic enrichment (including flavonoid-type constituents) in the ethyl acetate and butanol fractions. GC-MS captured volatile/non-polar features, while LC-HRMS covered semi-polar phenolics. Ethyl acetate showed the strongest DPPH scavenging (IC_{50} 23.9 µg/mL), whereas hexane exhibited the lowest cytotoxic IC_{50} (131.125 µg/mL) on MCF-7. Activity correlated with solvent polarity; phenolic-rich fractions displayed stronger antioxidant effects, while non-polar constituents aligned with greater whole-cell responses. Molecular docking qualitatively supported these trends by indicating stable interactions of representative phenolics within antioxidant-relevant sites. This work provides a first integrated link between fraction chemistry and bioactivity for *M. fragrans* leaves, highlighting the ethyl acetate fraction as a source of antioxidants and the hexane fraction as an antiproliferative-oriented lead. Limitations include a single cancer cell model and in silico inference; future isolation and mechanistic studies are warranted.

Keywords: Bioactivity, GC-MS, LC-HRMS, Molecular-docking, *Myristica fragrans*

Received: September 2025; Accepted: December 2025

Breast cancer remains a major contributor to global cancer morbidity and continues to motivate the identification of effective, low-toxicity bioactives. MCF-7 is a standard luminal model for antiproliferative screening. Oxidative stress contributes to carcinogenesis and therapy response, which justifies concurrent assessment of radical-scavenging capacity and cell viability when profiling plant extracts [1]. Nutmeg (*Myristica fragrans* Houtt.) leaves represent an underutilized biomass; valorization of leaf fractions aligns with bioprospecting and the circular bioeconomy of spices [2].

Myristica fragrans is rich in low-polarity volatiles and higher-polarity phenolics. Essential oil studies consistently report allylbenzenes and monoterpenoids as hallmark constituents, with eugenol-type phenylpropenes and myristicin among recurrent markers; antioxidant and anticancer activities have been documented [2, 3]. Quercetin modulates ROS, induces apoptosis, and suppresses proliferative signalling in MCF-7, and quercetin together with its metabolites inhibit xanthine oxidase, thereby providing a framework to interpret fraction-dependent antioxidant and cytotoxic readouts [4,5]. Complementary analytics are required to capture polarity-partitioned chemical space. Hexane fractions enriched in volatile or semivolatile constituents are amenable to GC-MS, whereas ethyl acetate and butanol fractions that concentrate phenolics and flavonoid glycosides benefit from LC-HRMS, which overcomes limitations of conventional LC-MS such as limited mass accuracy and coelution that hinder confident formula assignment and structural annotation, while providing high-accuracy mass detection and improved chromatographic resolution [6, 7, 8].

To couple annotation with function, in silico molecular docking is used as a hypothesis-generating bridge to evaluate whether major constituents can engage protein pockets implicated in oxidative-stress control and proliferative signalling, including Keap1, xanthine oxidase, ERα, and PI3Kα [9, 10, 11, 12]. Protocol validity is commonly supported by redocking co-crystallized ligands and a heavy-atom RMSD threshold of ≤ 2.0 Å as an accepted criterion for pose reproducibility [13]. The KEAP1–NRF2 literature delineates binding hotspots relevant to modulator design, and reference structures ERα LBD 3ERT and PI3Kα 4JPS provide pocket context for pose assessment [14, 15, 16].

A distinct gap remains, as only limited studies have simultaneously connected fraction-resolved chemistry of *M. fragrans* leaves (via GC-MS/LC-HRMS) with antioxidant and cytotoxic readouts and supportive docking within a single integrated framework. This study addresses that gap by mapping

the chemistry of hexane, ethyl acetate, and butanol fractions, quantifying antioxidant (DPPH) and antiproliferative (MCF-7) activities, and using docking to rationalize activity trends. The in silico findings are interpreted as preliminary mechanistic rationale requiring target-directed verification, and the practical outcome is the nomination of priority fractions and constituents for isolation and bioactivity evaluation.

EXPERIMENTAL

Chemicals and Materials

M. fragrans leaves served as the botanical source. High-purity solvents for extraction and partitioning included ethanol p.a, methanol p.a, hexane p.a, chloroform p.a, ethyl acetate p.a, and butanol p.a from Fulltime Chemical Co. (China), along with distilled water (laboratory grade). Analytical reagents and cell culture components comprised of 2,2-diphenyl-1-picrylhydrazyl (DPPH) and 3-(4,5-dimethylthiazol-2-yl)-2,5-diphenyltetrazolium bromide (MTT) from Merck (Germany), Fetal Bovine Serum (Corning, USA), the MCF-7 cell line, and DMSO, DMEM, and PBS (Merck, Germany). Equipment included a distillation set, a grinder, a rotary evaporator, standard laboratory glassware, capillary tubes, developing chambers, UV lamps, ovens, vials, analytical balances, separatory funnels, micropipettes, test tubes, Eppendorf tubes, a Biological Safety Cabinet, incubators, 96-well plates, a UV-Vis spectrophotometer, and a microplate reader. The selection of a graded polarity solvent system was intended to enable polarity-driven enrichment, allowing GC-MS profiling of the hexane fraction and LC-HRMS profiling of the ethyl acetate and butanol fractions with adequate chromatographic resolution and fragmentation pattern-based annotation; absorbance readouts at 517 nm for DPPH and 570 nm for MTT ensured reproducible bioactivity measurements.

Characterization Methods

Extraction Method

Dried *M. fragrans* leaves were milled and macerated in 70% v/v ethanol at ambient temperature under light protection for 72 h with intermittent agitation (≈5 min every 8 h). The solvent was refreshed every 24 h (3 x 24 h). All maceration filtrates were combined and evaporated under reduced pressure to obtain the ethanolic extract. The extract/combined filtrate was then resuspended in water and successively partitioned with n-hexane, ethyl acetate, and n-butanol (1:1 v/v, three washes each). Each organic phase was pooled, evaporated to dryness, weighed to calculate yield, and stored at 4°C in amber vials [17].

Phytochemical Screening

Each fraction (n-hexane, ethyl acetate, n-butanol) was dissolved in a polarity-matched solvent to 1–5 mg/mL and assayed at room temperature. Alkaloids were probed with Dragendorff's, Mayer's, and Bouchardat's reagents; phenolics with 1% $FeCl_3$ in ethanol; flavonoids by the Shinoda test (magnesium powder then 2 N HCl); tannins with 1% $FeCl_3$ in distilled water; terpenoids by the Liebermann-Burchard reaction; and saponins by the froth test. Readouts (color/ precipitate/foam) were evaluated within standard windows (precipitate ≤2 min, color ≤5 min, foam stability ≥1 min) and recorded as -/+/++. Each fraction-reagent combination was tested in triplicate with independently read by two blinded analysts. This qualitative screen served as preliminary mapping to guide downstream GC-MS/LC-HRMS [18].

Gas Chromatography-Mass Spectrometry (GC-MS) Analysis

The n-hexane fraction was analyzed on an Agilent 7890B/5977A with a DB-5MS UI column (30 m x 0.25 mm, 0.25 µm). He carrier at 1.0 mL min^{-1}; 1 µL splitless at 250°C. Oven: 40°C (1 min) to 300°C at 10°C min^{-1}, hold 7 min. EI 70 eV, m/z 30-600; transfer line/source/quadrupole 250/230/150°C. Peaks were tentatively assigned by NIST17 matches using TIC, RT, characteristic ions, and EI patterns. No derivatization was performed because the n-hexane fraction is dominated by non-polar, volatile constituents suitable for GC-MS [19].

Liquid Chromatography High-Resolution Mass Spectrometry (LC-HRMS) Analysis

Ethyl acetate and n-butanol fractions were profiled on a Thermo Orbitrap Exploris 120 with a ZORBAX Eclipse Plus C18 RRHD (2.1 x 100 mm, 1.8 µm). Mobile phases were 0.1% formic acid in water (A) and 0.1% formic acid in acetonitrile (B); 30-min run with a 95% A to 5% A gradient; 10 µL injection. ESI(+) full-scan m/z 100-1500 at 120k (m/z 200) with $ddMS^2$ at 60k (stepped HCD 18/35/53%). Data were processed in Compound Discoverer 3.3 with solvent-blank correction. For quality control, a standard solution appropriate to the ionization mode was injected before sample acquisition to verify instrument response and mass accuracy; daily and monthly calibrations were performed per the manufacturer protocol. Mass accuracy was maintained by the routine calibrations and pre-run verification.

Bioactivity Assays

Antioxidant

The radical-scavenging capacity of the hexane, ethyl acetate, and butanol fractions were assessed by the DPPH assay following [20], with minor adjustments. Precisely 4 mg of each fraction was dissolved in 4 mL of methanol and 750 µL of 0.1 mM DPPH in methanol was then added; the mixture was gently mixed and incubated for 30 min at room temperature in the dark. Methanol served as the negative control and quercetin

as the positive control. Post-incubation absorbance was read at 517 nm (Agilent Cary 60 UV-Vis). Radical-scavenging percentage was calculated as,

$$\% \text{ Inhibition} = [(A \text{ control} - A \text{ sample})/A \text{ control}] \times 100\%$$

The IC_{50} was derived from the logarithmic regression $y = a \ln(x) + b$ of % inhibition (y) versus concentration (x), yielding

$$x = \exp[(50 - b)/a]$$

Analytically, the key outputs are % inhibition at 517 nm and IC_{50}; the latter serving as a comparative metric of antioxidant potency (lower IC_{50} indicates stronger activity).

Antiproliferative

Human breast cancer MCF-7 cells were maintained in DMEM supplemented with 10% FBS and incubated at 37°C in 5% CO_2. Test fractions (hexane, ethyl acetate, and butanol) were dissolved in DMSO and applied at final concentrations of 400, 200, 100, 50, and 25 µg/mL, following the MTT protocol modified from [21]. Cells (1.5×10^4 per well) were seeded in 96-well plates, allowed to adhere for 24 h, and exposed to treatments for 48 h; then the media were aspirated and 10% MTT was added for 2 h. The MTT solution was removed, formazan crystals were dissolved with DMSO, cellular morphology was inspected microscopically, and absorbance was read at 570 nm using a microplate spectrophotometer.

$$\text{Cell viability (\%)} = [(OD \text{ sample} - OD \text{ blank}) / (OD \text{ control} - OD \text{ blank})] \times 100\%$$

IC_{50} values were estimated by probit regression of viability percentage versus the log of fraction concentration. The primary readouts were dose response curves, cell viability (%), and IC_{50}; these metrics quantify cytotoxic potency, with lower IC_{50} indicating stronger activity.

Molecular Docking

Three-dimensional conformations of myristicin and quercetin were obtained from PubChem (SDF), whereas (3β,5α,6α,15β,16β,24R)-stigmastane-3,6,8,15,16,29-hexol was built and energy-minimized in Avogadro (MMFF94s; conjugate gradients) to convergence. All ligands were exported to PDB in BIOVIA Discovery Studio 2025. Protein structures ERα LBD (3ERT), PI3Kα (4JPS), Keap1 Kelch (5FNU), and xanthine oxidase (3NVY) were downloaded from the RCSB PDB; water and heteroatoms were removed, co-crystallized ligands were retained as references for redocking and active-site definition, and any missing residues were repaired in Swiss-PdbViewer. Receptors were prepared in PyRx (Make Macromolecule). Ligands were processed via Open Babel in PyRx and converted to PDBQT for AutoDock Vina. Docking in PyRx used grids centerd on native ligands with dimensions specified in Table Grid Dock, returning binding free energies and ranked poses. The protocol was validated by redocking native ligands and computing heavy-atom RMSD in PyMOL (rms_cur) against crystallographic poses; RMSD ≤ 2.0 Å was accepted as the reliability criterion [22,13]. Protein-ligand interactions were inspected in two- and three-dimensional views using BIOVIA Discovery Studio Visualizer.

Statistical Analysis

Results are reported as mean ± standard deviation (SD). Group comparisons were performed using one-way analysis of variance (ANOVA) and, where the omnibus test indicated significance, Tukey's post-hoc multiple-comparison test was applied; two-tailed p-values < 0.05 were considered statistically significant. All computations were conducted in Minitab.

RESULTS AND DISCUSSION

The phytochemical screen of the hexane, ethyl acetate, and butanol fractions (**Table 1**) indicate a polarity-driven partition of secondary metabolites. Hexane shows terpenoids with a minor phenolic signal and no detectable flavonoids, whereas ethyl acetate presents the broadest profile with strong phenolics and flavonoids plus lower tannins, terpenoids, and saponins; butanol retains strong phenolics with moderate flavonoids and terpenoids. From 2.0 kg of dried leaves we obtained 374 g of crude extract (18.70%), and 340 g of this extract was fractionated to yield 18.5 g (5.44%) hexane, 36.6 g (10.76%) ethyl acetate, and 71.3 g (20.97%) butanol of the fractionated extract, or 0.93%, 1.83%, and 3.57% relative to the dried leaves, respectively; the three fractions account for 126.4 g in total (37.18% of the fractionated extract). This distribution follows solubility principles in which non-polar solvents extract non-polar constituents, and semi-polar or polar solvents enrich medium-to-high polarity metabolites. The screen is qualitative and intended as initial mapping to direct instrument choice; hexane is best interrogated by GC-MS for non-polar markers, while ethyl acetate and butanol warrant LC-HRMS to secure chromatographic resolution of phenolics, tannins, and flavonoid glycosides [23, 24]. Quantitative compositional trends are addressed in the GC-MS/LC-HRMS sections.

Chemical Composition

Reports on nutmeg seeds consistently highlight allylbenzenes and terpenoids as dominant non-polar volatiles, whereas leaves show comparatively higher levels of phenolics and flavonoid-type constituents. This seed-leaf contrast aligns with our fractionation pattern, where hexane captured non-polar markers and ethyl acetate-butanol concentrated phenolic

features [2, 32]. Hexane is dominated by oxygenated phenylpropanoids and neolignans, consistent with *M. fragrans* volatiles; ethyl acetate concentrates flavonols and their glycosides; butanol is enriched in phytosterol- and glycolipid-type features. GC-MS of hexane revealed 12 dominant constituents totalling 60.38% TIC (**Figure 1; Table 2**), led by phenylpropanoids (myristicin, elemicin, dimethoxyeugenol, *trans*-isoeugenol; 25.86%) and neolignans (14,41%), with additional FAME (9.73%), isoprenoids (8,29%), and oxygenated monoterpenes (2.09%). LC-HRMS of ethyl acetate yielded high-confidence features with mzCloud confidence ≥ 95% and low-ppm exact-mass agreement, assigned as quercetin (99.8%), taxifolin (98.7%), quercitrin (97.8%), hyperoside (97.7%), and afzelin (98.3%) (**Table 3**), supported by diagnostic product-ion patterns. LC-HRMS of butanol, under stringent QC (mass accuracy ≤ 5 ppm; peak quality ≥ 7.5), retained stigmastane-hexol ($C_{29}H_{52}O_6$; RT 19.75 min) and several lipid-derived and N-acyl-hexosamine glycolipids (**Table 4**) with corroborative MS/MS fragments.

Table 1. Phytochemical screening of hexane, ethyl acetate, and butanol fractions.

Phytochemical Group	Test Reagents	Observable Reaction	Hx (n=3x2)	EA (n=3x2)	Bu (n=3x2)
Alkaloids	Dragendorff's/ Mayer's/ Borchadart	Orange-brown/ White-yellow/ Brown ppt	− (0/6)	− (0/6)	− (0/6)
Phenolics	Ethanol+$FeCl_3$	Deep blue, green or black coloration	+ (4/6)	++ (6/6)	++ (6/6)
Flavonoids	2N HCl + Magnesium powder	Red or orange-red coloration	− (0/6)	++ (5/6)	+ (4/6)
Tannins	Distilled water + 1% $FeCl_3$	Greenish purple coloration	− (0/6)	+ (3/6)	− (1/6)
Terpenoids	Acetic acid + Concentrated H_2SO_4	Color change from dark blue to green	++ (6/6)	+ (3/6)	+ (3/6)
Saponins	Heating, shaking + 2N HCl	Formation of stable foam	− (0/6)	+ (3/6)	− (1/6)

*Hx = n-hexane, EA = ethyl acetate, Bu = n-butanol. Symbols denote the modal qualitative call (−/+/++) across two blinded analysts and three technical replicates per fraction; values in parentheses indicate the number of positive calls out of six reads (analyst x replicate). Readout windows were standardized (precipitate ≤2 min, color ≤5 min, foam stability ≥1 min).

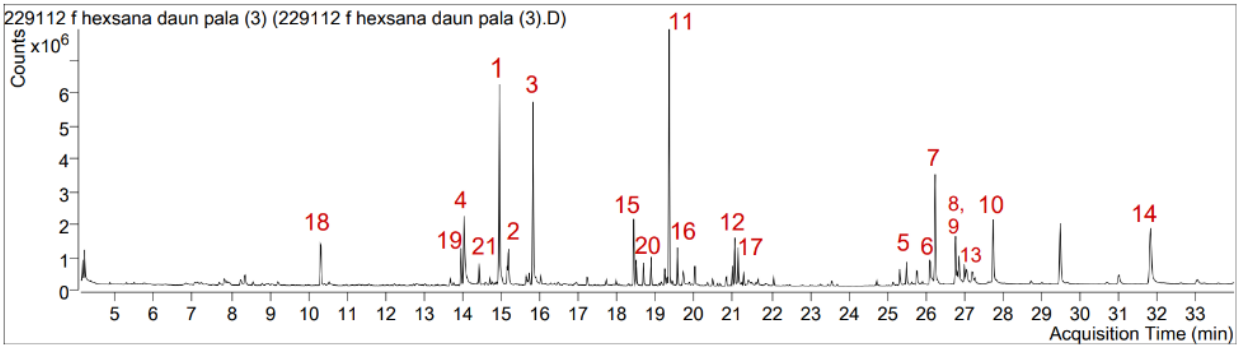

Figure 1. Total ion chromatogram (TIC) of the hexane leaf fraction (GC-MS)

*X-axis: acquisition time (min). Y-axis: TIC intensity (counts ×10^6). Major peaks are visually labelled 1-21 at the apex and correspond to the compounds listed in Table 2. Highlighted peaks were shortlisted by largest area contribution and Qual (reverse-match) >90%

The GC-MS suite matches known *M. fragrans* volatiles and semi volatiles, where allylbenzenes and monoterpenoids mark *Myristica fragrans* [2]. Tocopherols and phytol-type isoprenoids stabilize lipid phases and limit peroxidation, potentially adding to antioxidant tone [25]. In LC-HRMS, aglycone masses, neutral-loss signatures, and fragmentation patterns rationalize the annotation of flavonoid glycosides (**Table 4; Table 5**). The composition aligns with prior *M. fragrans* reports for allylbenzenes and monoterpenoid oxygenates and with LC-MS rules of thumb for flavonoids and their glycosides [2, 26, 27].

Table 2. Dominant compounds in the hexane fraction by GC-MS analysis.

No	Compound IUPAC (Trivial)	Formula	RT	Area (%)
Phenylpropanoids				
1	4-Methoxy-6-(2-propen-1-yl)-1,3-benzodioxole (**myristicin**)	$C_{11}H_{12}O_3$	14.95	9.17
2	1,2,3-Trimethoxy-5-(2-propen-1-yl)benzene (**elemicin**)	$C_{12}H_{16}O_3$	15.19	2.76
3	2,6-Dimethoxy-4-(2-propen-1-yl)phenol (**dimethoxyeugenol**)	$C_{11}H_{14}O_3$	15.82	8.39
4	(*E*)-2-Methoxy-4-(1-propenyl)phenol (***trans*-isoeugenol**)	$C_{10}H_{12}O_2$	14.04	5.54
Neolignans				
5	(*S*)-5-Allyl-1,3-dimethoxy-2-((1-(3,4,5-trimethoxyphenyl)propan-2-yl)oxy)benzene	$C_{23}H_{30}O_6$	26.24	5.67
6	(1*S*,2*R*)-2-(4-Allyl-2,6-dimethoxyphenoxy)-1-(3,4-dimethoxyphenyl)propyl acetate	$C_{24}H_{30}O_7$	26.77	2.3
7	4-[2-(2,6-Dimethoxy-4-prop-2-enylphenoxy)-1-hydroxypropyl]-2-methoxyphenol	$C_{21}H_{26}O_6$	26.86	2.36
8	(1*S*,2*R*)-2-(4-Allyl-2,6-dimethoxyphenoxy)-1-(3,4,5-trimethoxyphenyl)propan-1-ol-rel-	$C_{23}H_{30}O_7$	27.76	4.08
Fatty acids & esters				
9	Hexadecanoic acid, methyl ester (**palmitic acid, methyl ester**)	$C_{17}H_{34}O_2$	19.36	9.73
Isoprenoids				
10	3,4-Dihydro-2,5,7,8-tetramethyl-2-(4,8,12-trimethyltridecyl)-2*H*-1-benzopyran-6-ol (**DL-*α*-Tocopherol**)	$C_{29}H_{50}O_2$	31.83	5.7
11	7,11,15-Trimethyl-3-methylene-1-hexadecene (**neophytadiene**)	$C_{20}H_{38}$	18.44	2.59
Oxygenated monoterpenes				
12	4-Methyl-1-(1-methylethyl)-3-cyclohexen-1-ol (**Terpinen-4-ol**)	$C10H_{18}O$	10.33	2.09
	Total			60.38%

Table 3. Dominant compounds in the ethyl acetate fraction by LC-HRMS analysis.

No	Compound	RT (min)	Area Max	Measured (m/z)	Exact mass	Product ions (m/z)	Group
1	Quercetin	11.878	42.36 x 10^7	303.04	302.04	285.04; 257.04; 229.05; 201.05; 153.08; 121.02	Flavonoid
2	Taxifolin	6.506	21.63 x 10^7	305.06	304.05	287.05; 259.06; 241.05; 213.05; 153.01; 121.03	Flavonoid
3	Quercitrin	6.786	15.43 x 10^7	449.10	448.10	303.05; 287.05; 229.05; 159.22; 137.02	Flavonoid glycoside
4	Hyperoside	6.341	14.71 x 10^7	465.10	464.09	303.05; 285.04; 257.04; 229.05; 153.02	Flavonoid glycoside
5	Afzelin	7.253	2.87 x 10^7	433.112	432.10	287.05; 258.05; 213.05; 165.02; 153.02	Flavonoid glycoside

Table 4. Dominant compounds in the butanol fraction by LC-HRMS analysis.

No	Compound	RT (min)	Area Max	Measu-red (m/z)	Exact mass	Product ions (m/z)	Group
1	(3β,5α,6α,15β,16β,24R)-Stigmastane-3,6,8,15,16,29-hexol	19.75	14.22 x 10^7	514.41	496.37	181.08; 245.11; 263.12; 273.12; 291.12; 309.13; 365.19	Steroid (Phytosterol)
2	(6R)-6-[(2S,4S,7S)-2,4,7-Trihydroxyhenicosyl]-5,6-dihydro-2H-pyran-2-one	20.2	7.692 x 10^7	441.35	440.35	181.08; 199.09; 230.64; 257.02; 312.22; 350.75	Lipid-derived
3	Hexadecyl 2-deoxy-2-(4-pentenoylamino)-α-D-glucopyranoside	17.48	5.51 x 10^7	486.37	485.37	163.11; 191.10; 209.11; 237.11; 255.12; 293.17; 311.18; 329.19; 423.31; 441.32	Glycolipid
4	2-Deoxy-2-(palmitoylamino)-D-glucopyranose	15.95	4.29 x 10^7	418.31	417.31	171.13; 185.11; 196.23; 228.40; 273.59; 295.92; 367.41; 375.95	Glycolipid
5	(2S,3R)-2-(Hydroxymethyl)-5-oxotetrahydro-3-furanyl nonadecanoate	18.43	4.15 x 10^7	413.32	412.32	181.12; 209.11; 227.12; 255.19; 284.19; 339.25	Lipid-derived

Table 5. Chemical formulae and MS/MS spectra of dominant compounds in the ethyl acetate fraction.

No	MS spectra	Structure
1	Quercetin ($C_{15}H_{10}O_7$)	

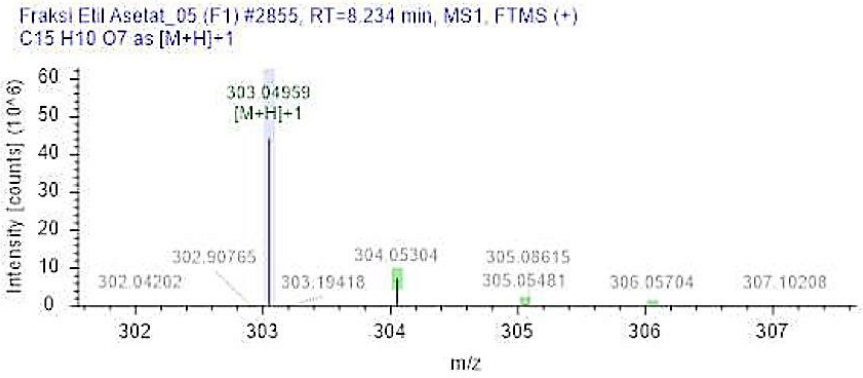

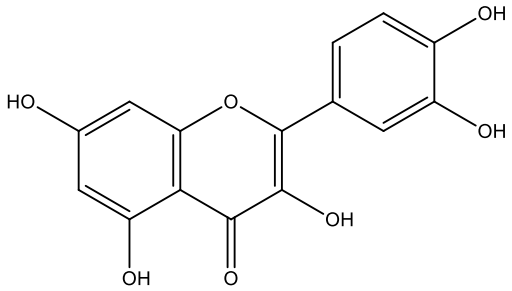

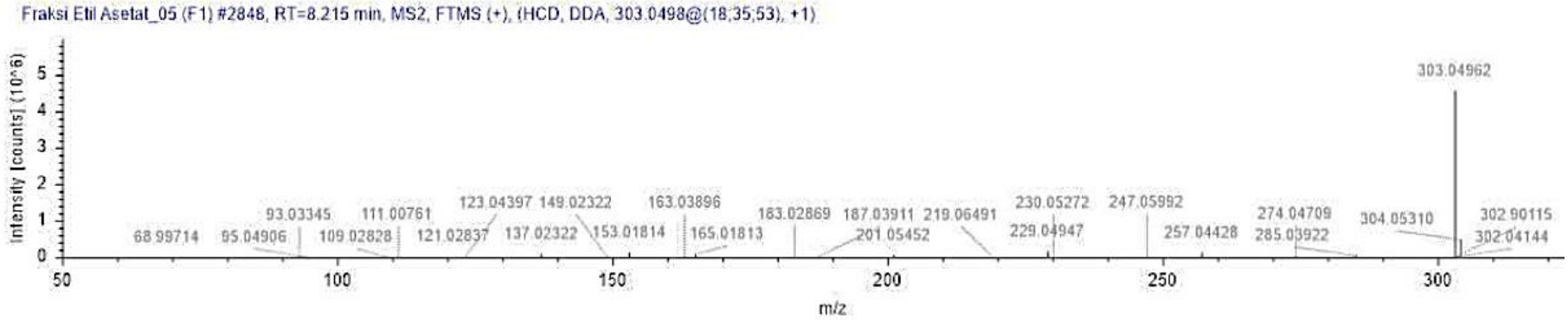

2 Taxifolin ($C_{15}H_{12}O_7$)

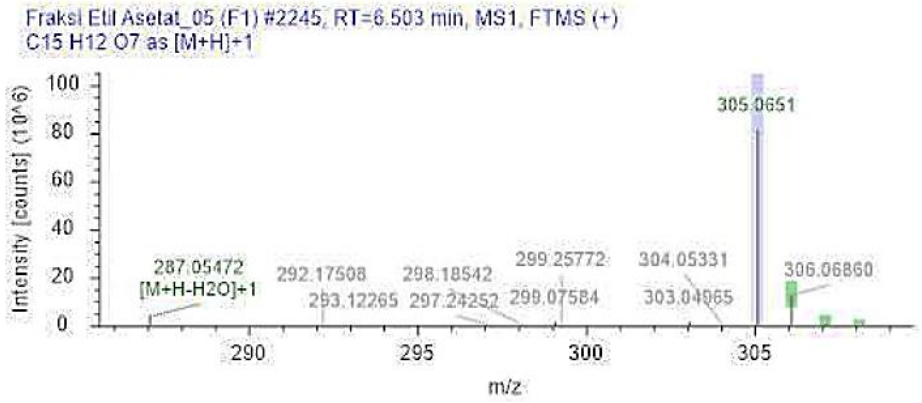

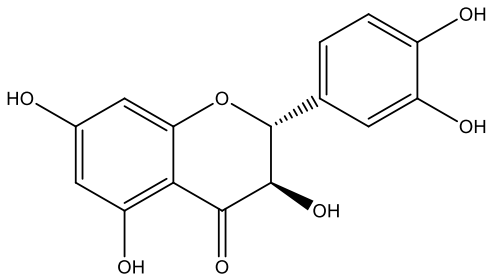

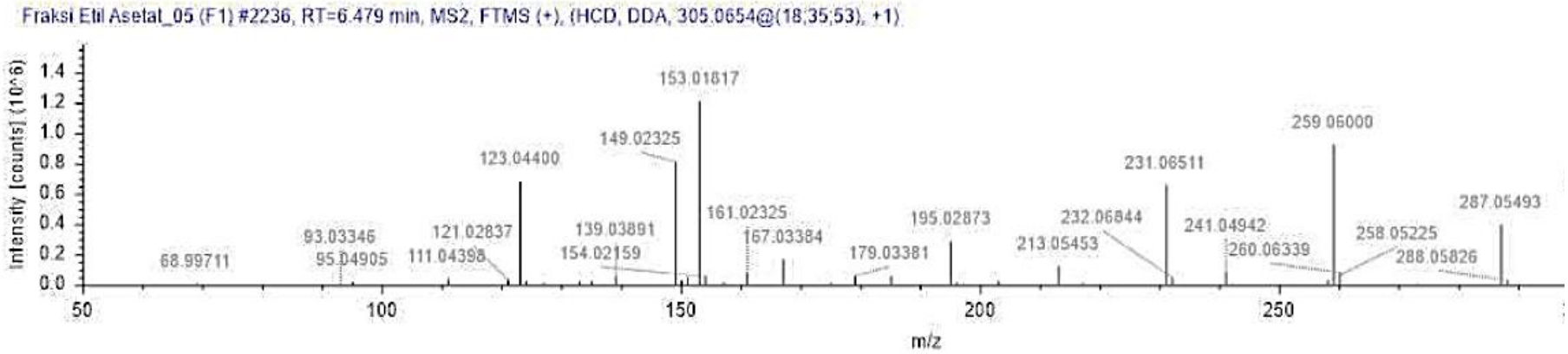

3 Quercitrin ($C_{21}H_{20}O_{11}$)

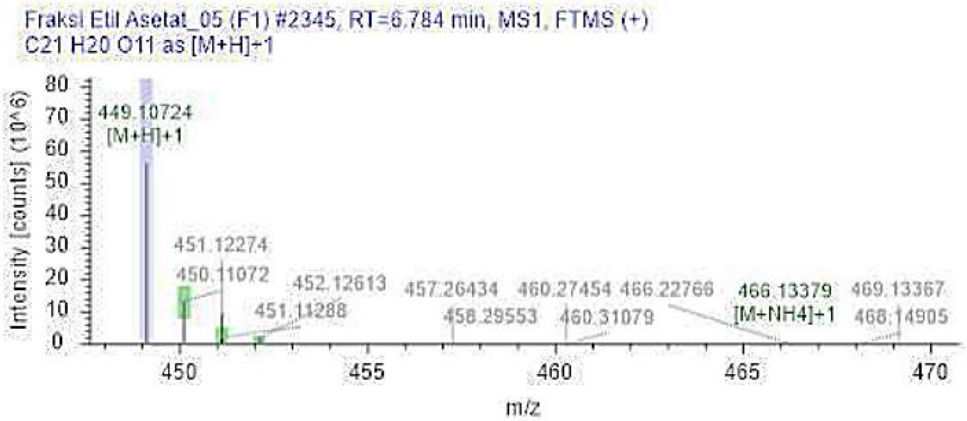

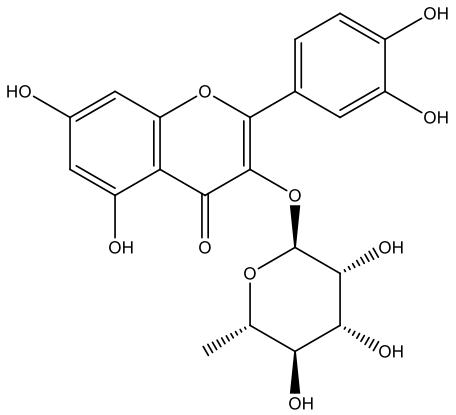

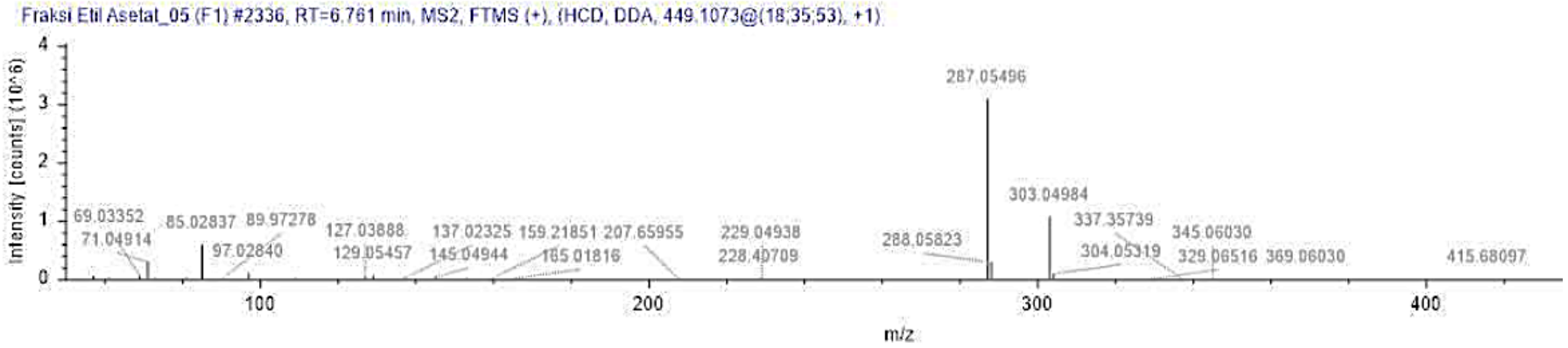

4 Hyperoside ($C_{21}H_{20}O_{12}$)

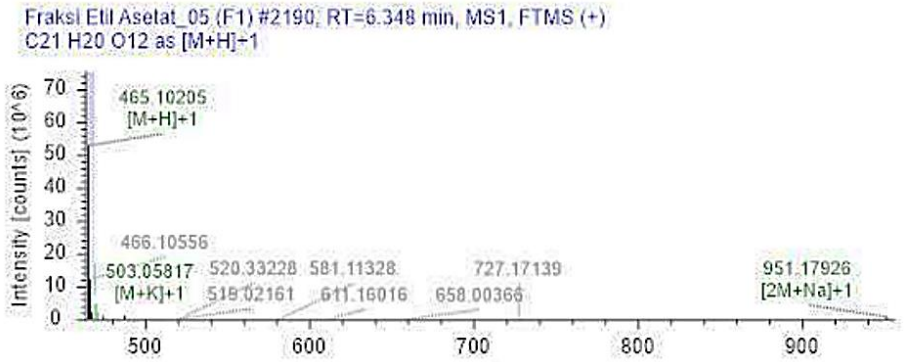

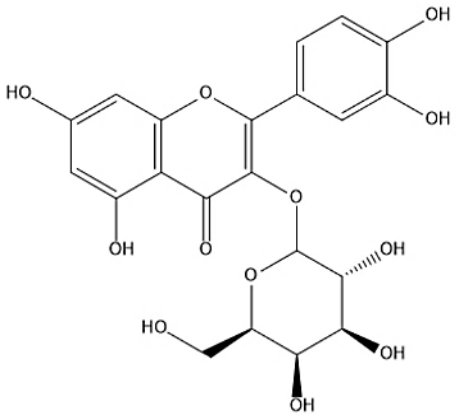

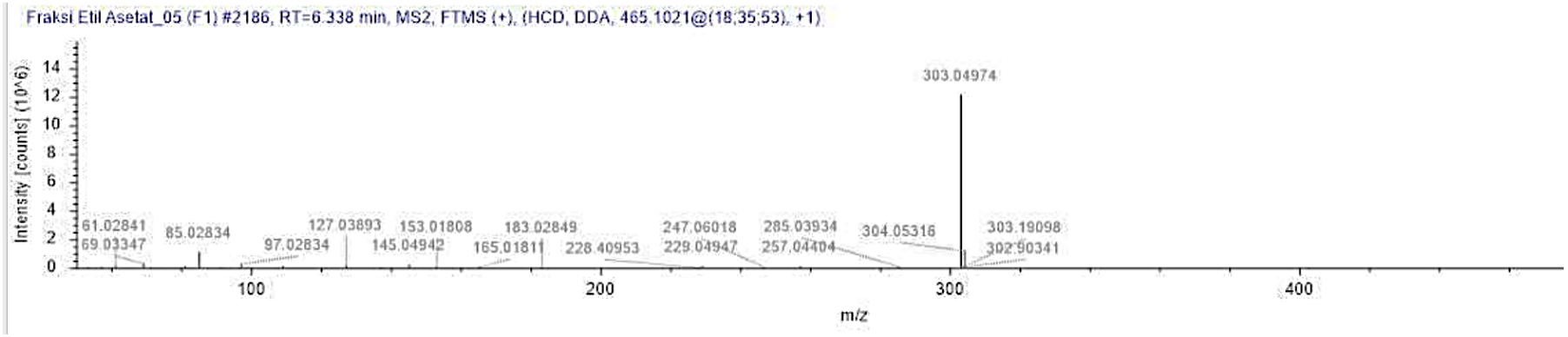

5 Afzelin ($C_{21}H_{20}O_{10}$)

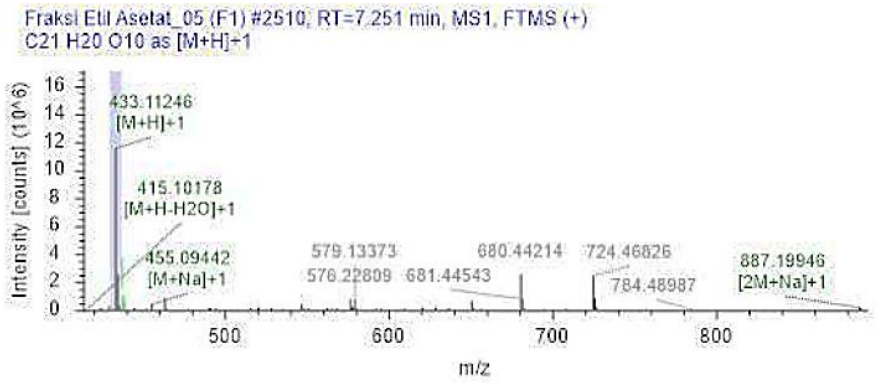

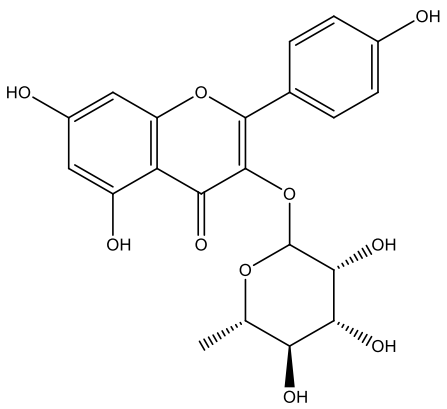

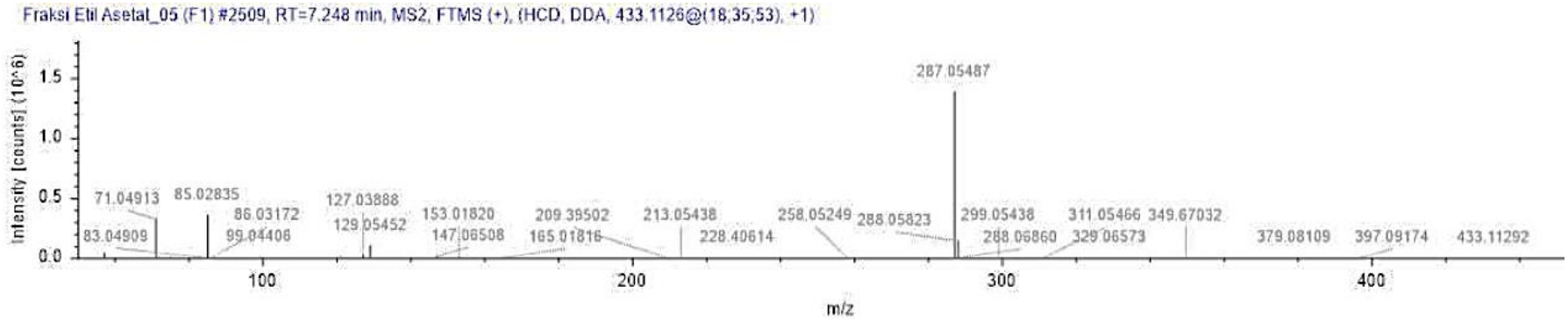

Table 6. Chemical formulae and MS/MS spectra of dominant compounds in the butanol fraction.

No	MS spectra	Structure
1	(3β,5α,6α,15β,16β,24R)-Stigmastane-3,6,8,15,16,29-hexol ($C_{29}H_{52}O_6$)	

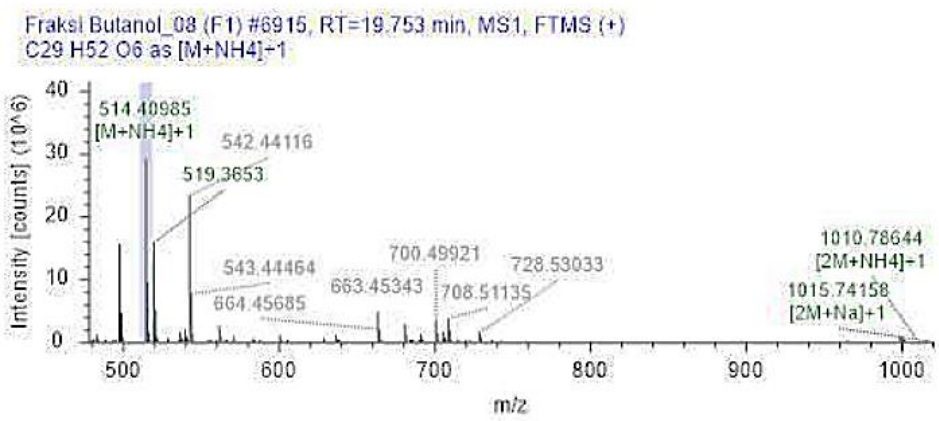

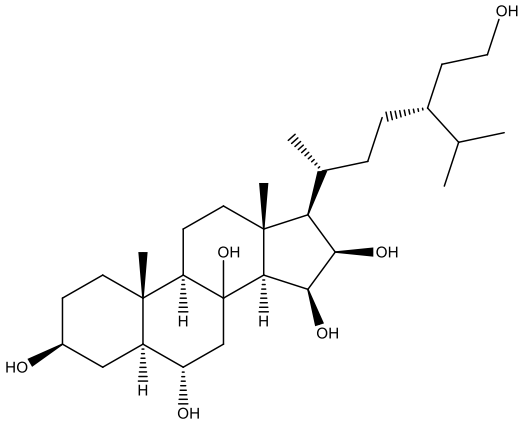

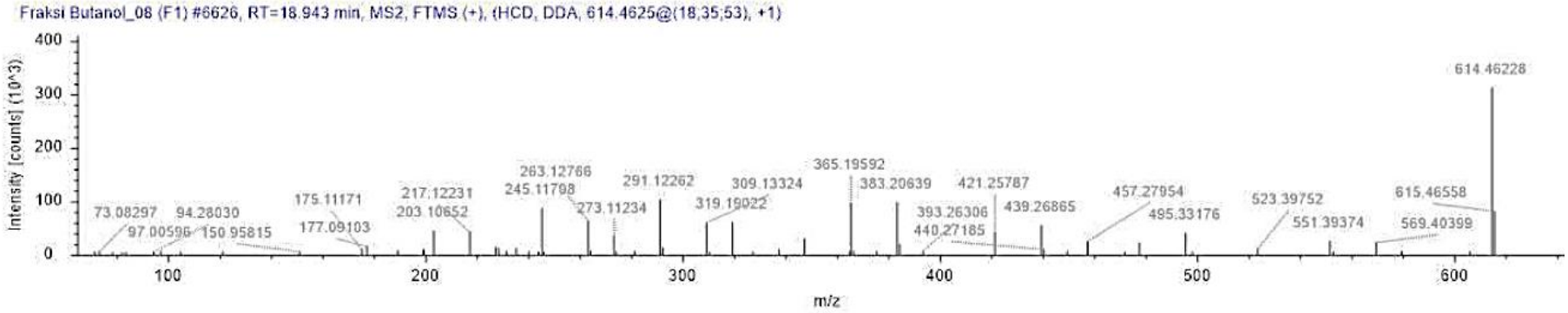

2 (6R)-6-[(2S,4S,7S)-2,4,7-Trihydroxyhenicosyl]-5,6-dihydro-2H-pyran-2-one ($C_{26}H_{48}O_5$)

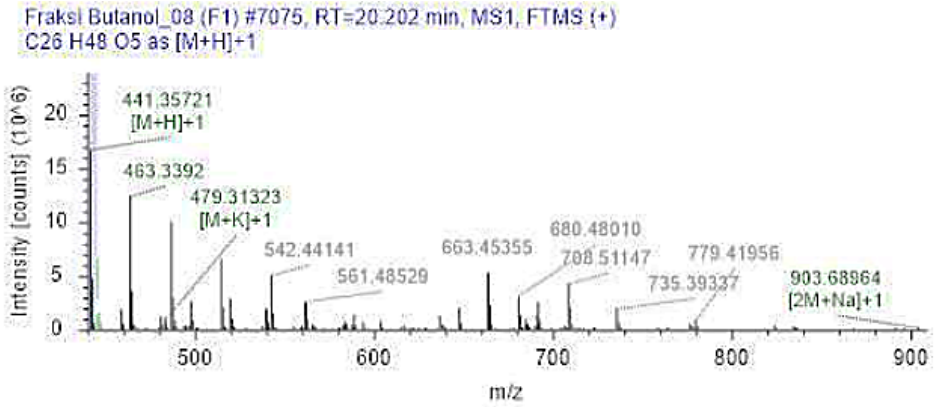

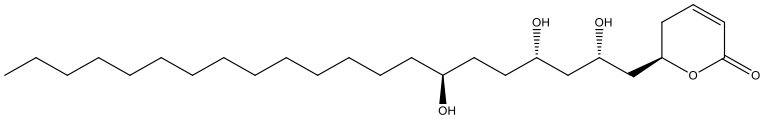

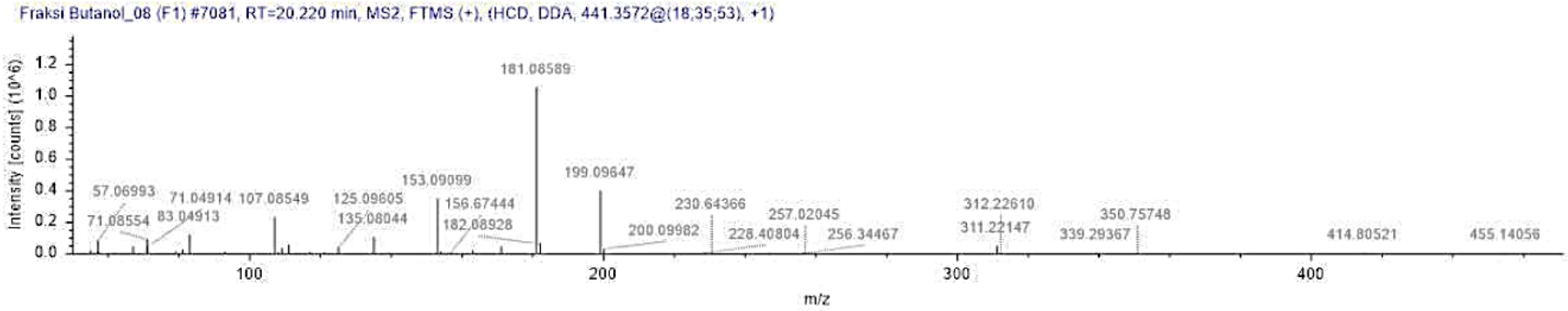

3 Hexadecyl 2-deoxy-2-(4-pentenoylamino)-α-D-glucopyranoside ($C_{27}H_{51}NO_6$)

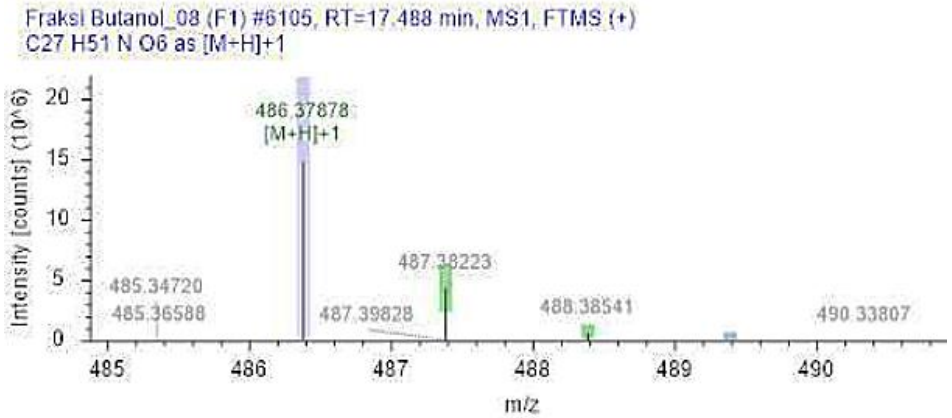

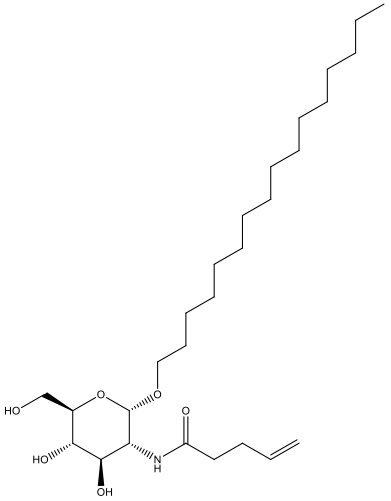

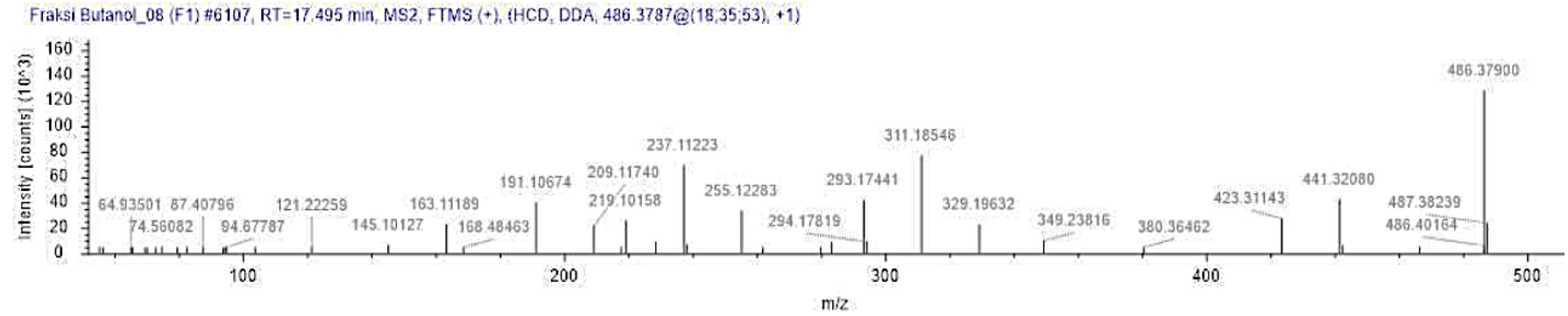

4 2-Deoxy-2-(palmitoylamino)-D-glucopyranose ($C_{22}H_{43}NO_6$)

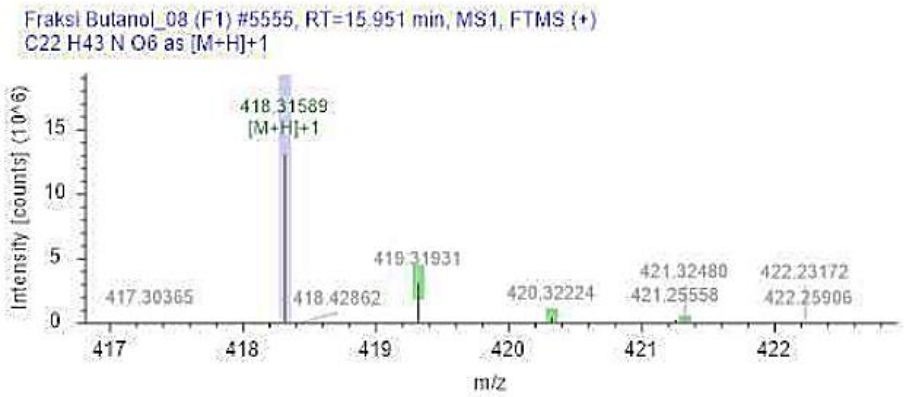

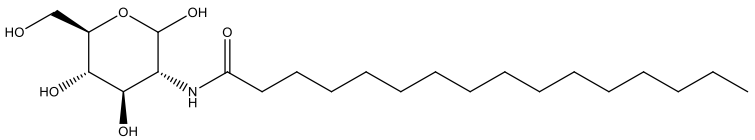

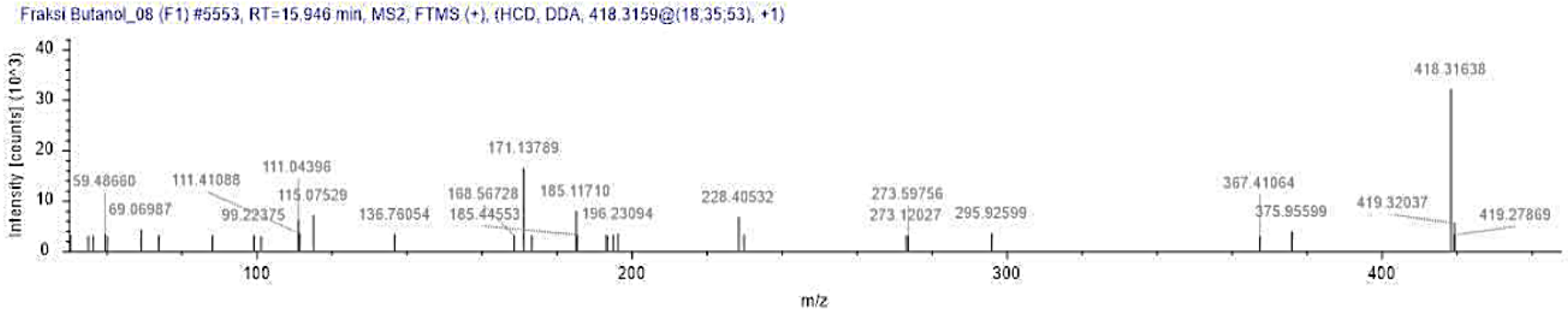

(2S,3R)-2-(Hydroxymethyl)-5-oxotetrahydro-3-furanyl nonadecanoate ($C_{24}H_{44}O_5$)

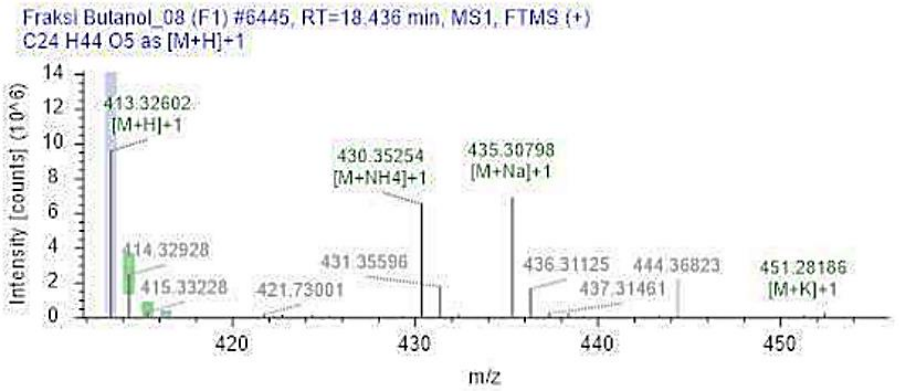

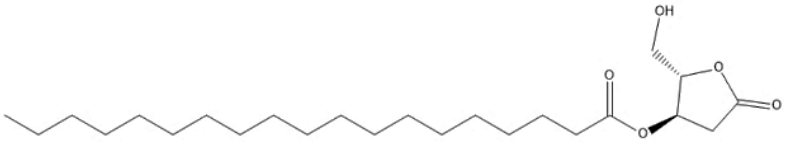

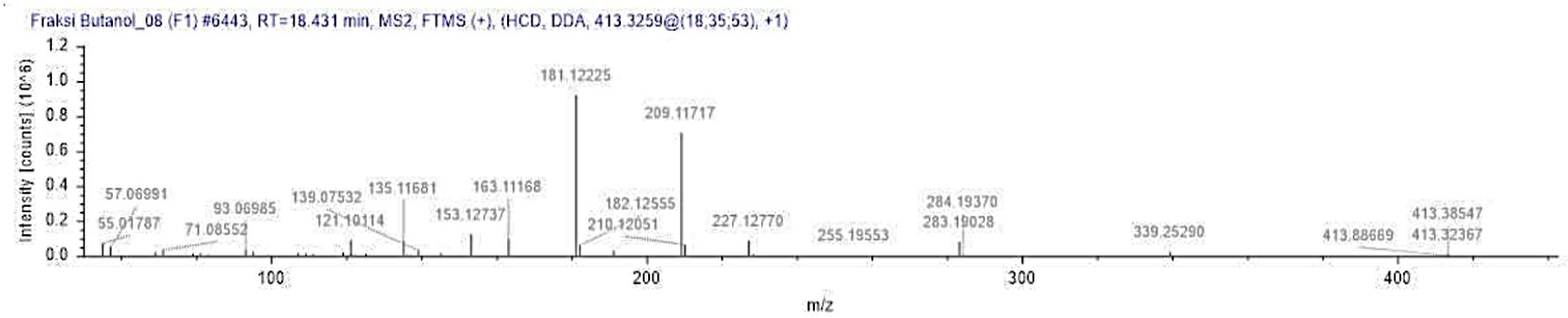

Antioxidant Activity (DPPH)

Ethyl acetate shows the strongest radical-scavenging capacity. IC_{50} values (mean ± SD, n = 3) were ethyl acetate 23.92 ± 2.75 µg/mL, hexane 44.86 ± 0.38 µg/mL, and butanol 104.22 ± 5.05 µg/mL; ethyl acetate < hexane < butanol ($p < 0.05$) (**Table 7**). Using the referenced classification, ethyl acetate and hexane fall in the very strong category (< 50 µg/mL), while butanol is moderate [28]. The ethyl acetate fraction shows the strongest DPPH activity, consistent with its detected phenolics, including flavonoid aglycones and glycosides. Chemically, phenolics are efficient H/e^- donors and their resulting phenoxyl radicals are resonance-stabilized. This explains why phenolic-rich fractions tend to give lower DPPH IC_{50} values [29]. Higher IC_{50} for butanol likely reflects co-extraction of sugars and highly glycosylated species that attenuate aglycone reactivity; hexane's activity probably derives from lipophilic antioxidants that stabilize radical intermediates but typically underperform polyphenols in this assay [30,17,31].

External consistency appears with a methanolic leaf extract (IC_{50} 36.31 µg/mL; vitamin C 3.657 µg/mL) and multi-assay evidence indicating high TPC and antioxidant capacity in acetone extracts [32,33]. A targeted hexane subfraction (MFHD-4) reached IC_{50} of 0.729 µg/mL, outperforming vitamin C of 7.875 µg/mL, underscoring fractionation effects [34]. DPPH is a chemical endpoint and does not model cellular redox flux; phenolic speciation should be linked to cellular assays in future work.

Antiproliferative Activity (MCF-7, MTT)

Hexane exhibits the strongest antiproliferative effect against MCF-7. In MCF-7 cells, the hexane fraction produces the greatest loss of viability, consistent with a dominance of non-polar constituents that can interact with cell membranes and influence the MTT readout. The ethyl acetate fraction shows intermediate effects, whereas the butanol fraction is weakest. This pattern is reasonable given differences in polarity, permeability, and the likelihood that the most polar fraction contains more inert matrix components [35,36]. Viability decreased with dose, ranking hexane > ethyl acetate > butanol. At 400 µg/mL, viability was 10.29%, 14.85%, and 32.16%, respectively (**Table 8**; n = 3). Two-way ANOVA detected significant main effects of fraction and concentration and a significant interaction (global $p < 0.0001$), with most pairwise Tukey comparisons significant at $p < 0.05$. IC_{50} values corroborated the ranking, hexane 131.125 µg/mL, ethyl acetate 181.301 µg/mL, and butanol 307.542 µg/mL. According to NCI thresholds [37], hexane and ethyl acetate are classified as moderate, whereas butanol is low.

Table 7. Antioxidant activity of hexane, ethyl acetate, and butanol fractions.

Fractions	IC_{50} (µg/mL)
hexane	44.86 ± 0.38
ethyl acetate	23.92 ± 2.75
butanol	104.22 ± 5.05

*Data are expressed as mean ± SD, n = 3. One-way ANOVA followed by Tukey's test showed that the ethyl acetate fraction had a significantly lower IC_{50} value ($p < 0.05$), indicating the highest antioxidant activity among the fractions.

Table 8. Inhibitory activity of hexane, ethyl acetate, and butanol fractions against MCF-7 breast cancer cell.

Fractions		Concentration				
		25	50	100	200	400
Hexane	Absorbance	1.068 ±0.048	0.955 ±0.005	0.660 ±0.043	0.391 ±0.006	0.144 ±0.005
	Viability	76.18 %	68.14 %	47.11 %	27.90 %	10.29 %
Ethyl Acetate	Absorbance	1.266 ±0.01	1.102 ±0.007	0.791 ±0.004	0.492 ±0.005	0.208 ±0.004
	Viability	90.30 %	78.60 %	56.40 %	35.08 %	14.85 %
Butanol	Absorbance	1.303 ±0.014	1.259 ±0.078	1.158 ±0.044	1.044 ±0.101	0.451 ±0.04
	Viability	89.94 %	85.02 %	82.62 %	74.47 %	32.16 %

*Data are expressed as mean ± SD, n = 3. Two-way ANOVA revealed that fraction type and concentration significantly affected cell viability ($p < 0.0001$). A significant interaction was also observed between fraction and concentration ($p < 0.0001$), indicating that the effect of concentration depends on the fraction used. Tukey's post-hoc test identified that most group pairwise comparisons were statistically significant ($p < 0.05$).

The hexane fraction likely concentrates membrane-active, lipophilic constituents that impair mitochondrial dehydrogenase activity, lowering MTT reduction; phenolics in ethyl acetate show intermediate effects, with glycosylation limiting permeability and shifting outcomes towards cytostatic effects; high polarity in butanol co-extracts inert matrices or heavily glycosylated species that further blunt activity [38,39,17]. The pattern aligns with prior *M. fragrans* literature showing MCF-7 activity for essential oil and cytotoxic signals from hexane root extracts and bark-derived constituents [3,40,41].

Molecular Docking

The docking workflow is reliable and supports quercetin as the most consistent binder across the selected targets. Redocking RMSD values were ≤ 2.0 Å for Keap1 5FNU 0.355 Å, XO 3NVY 1.074 Å, ERα 3ERT 1.400 Å, and PI3Kα 4JPS 0.700 Å (**Table 9**), meeting accepted criteria [42,43]. Docking was used to provide mechanistic context for the assays, with one representative ligand from each fraction (myristicin for hexane, quercetin for ethyl acetate, stigmastane-hexol for butanol) alongside target-specific reference ligands. The outcomes qualitatively align with the experiments: the phenolic representative engages sites relevant to indirect antioxidant control, while the lipophilic representative fits hydrophobic pockets yet does not surpass reference ligands at targets requiring polar anchoring. Because each test ligand represents a single dominant component from a complex fraction, docking conclusions are interpreted as fraction-level mechanistic support rather than proof of single-compound activity.

Against Keap1 5FNU, KI-696 (native ligand) scored ΔG of -11.8 kcal/mol with Arg415, Ala556, Tyr525; quercetin and stigmastane-hexol each scored -8.9 kcal/mol, with quercetin contacting Arg415/ Ala556 and the sterol occupying hydrophobic subpockets; myristicin was weaker at -6.0 kcal/mol. These trends agree with structure–activity relationship expectations in which anchoring at Arg415 and productive hydrophobic complementarity enhance complex stabilization in Keap1 [14,44,45]. In XO 3NVY, febuxostat (ref.) scored -8.4 kcal/mol, quercetin -7.5, stigmastane-hexol -6.3, and myristicin -5.6. For ERα 3ERT, 4-hydroxytamoxifen scored -9.5 kcal/mol, with hinge contacts at Glu353; quercetin -7.9 with retained Glu353 interactions, whereas myristicin -6.2 and stigmastane-hexol -5.5 with lacked directional donors [46,47]. In PI3Kα 4JPS, alpelisib scored -10.3 kcal/mol with contacts at Lys802, Ile848, Val851, Ser854, and Met922; quercetin -8.4 and stigmastane-hexol -8.1 and were compatible with the ATP pocket but lacked hinge anchoring; and myristicin -6.4 was the weakest [48].

Quercetin combines hydrogen-bonding capacity with aromatic planarity, enabling stable interactions at canonical hotspots; the bulky sterol benefits from hydrophobic complementarity in Keap1 but loses advantage where directional donors are required; myristicin's small, low-polarity scaffold limits polar contacts and yields peripheral binding. These trends mirror reports on Keap1-Nrf2 modulators, XO flavonoid inhibition, ERα recognition, and PI3Kα selectivity [14,49,50]. Docking is predictive and does not replace biochemical confirmation.

Across chemical profiling and bioassays, ethyl acetate emerges as a phenolic-rich antioxidant source with very-strong DPPH activity, whereas hexane concentrates nonpolar entities associated with the strongest MCF-7 growth inhibition. Docking rationalizes these patterns by identifying quercetin as a multi-target binder, a sterol that fits Keap1 hydrophobics, and myristicin as a weaker ligand. The main limitations are qualitative phytochemical screening, the chemical nature of DPPH, and the predictive status of docking; prioritized next steps include isolation and orthogonal validation of quercetin- and sterol-type constituents and mechanistic assays on redox and apoptotic signalling.

Table 9. Docking interaction of protein selected with native ligand, myristicin (Hx fraction), quercetin (EA fraction), and stigmastane-hexol (Bu fraction).

Compound	Binding affinity (kcal/mol)	Interaction	2D	3D
Antioxidant (5FNU) RMSD : 0.355 Å				
Native ligand (KI696)	-11.8	Asn382, Asn414, Arg415, Gly462, Gly509, Tyr525, Ser555, Ala556	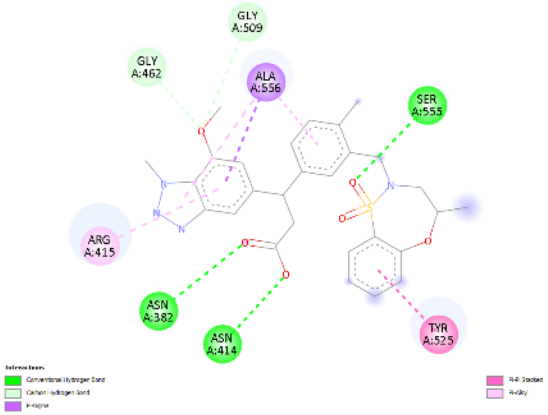	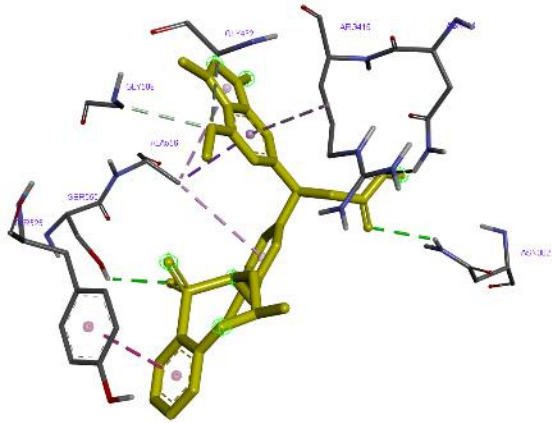
Myristicin	-6.0	Arg483, Ser508, Tyr525, Tyr572	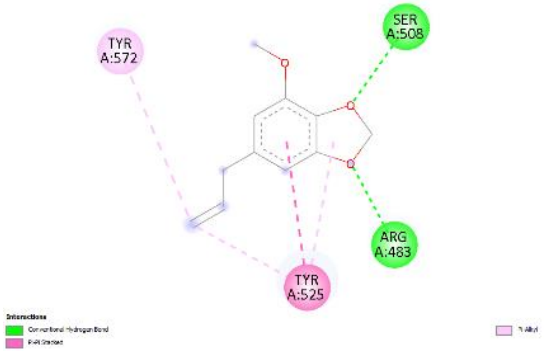	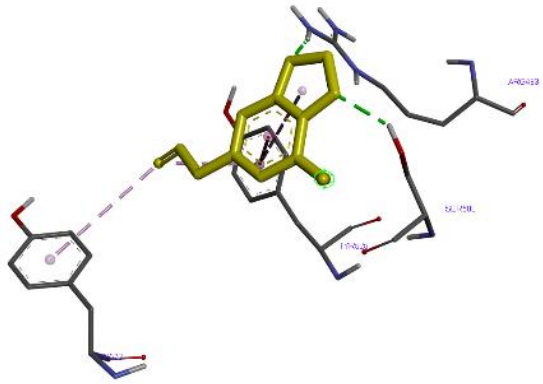

Quercetin	-8.9	Ala366, Arg415, Val463, Gly464, Val465, Val512, Ala556	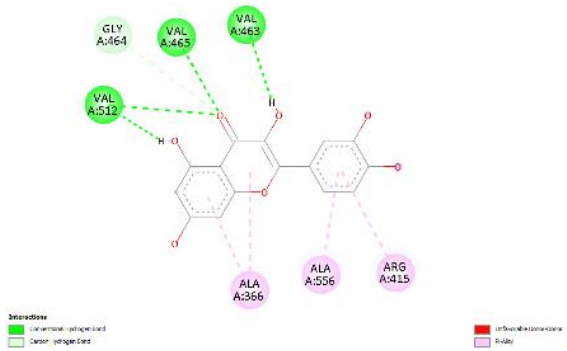	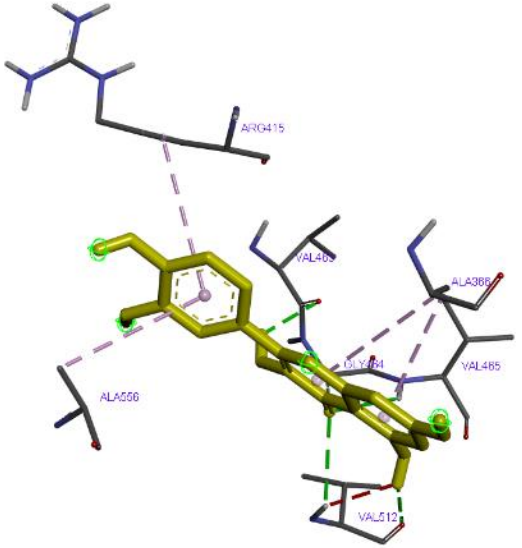
Stigmastane-hexol	-8.9	Arg415, Val463, Val465, Arg483, Ala556, Val606	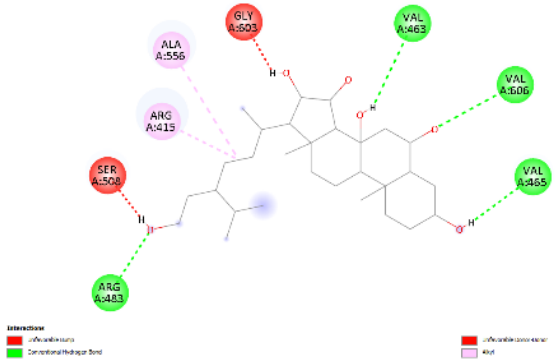	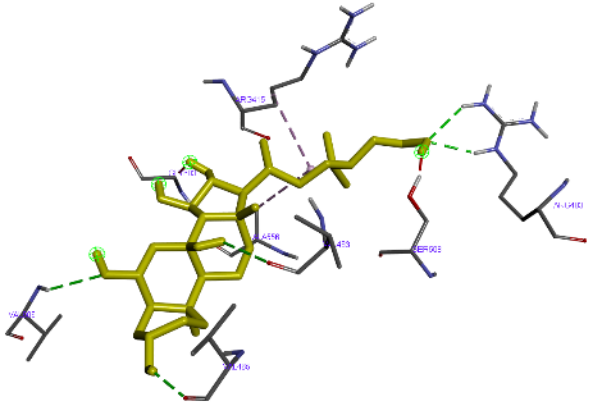

Antioxidant (3NVY) RMSD : 1.074 Å				
Native ligand (Quercetin)	-7.5	Leu648, Leu873, Ser876, Arg880, Phe914, Val1011, Leu1014, Ala1079	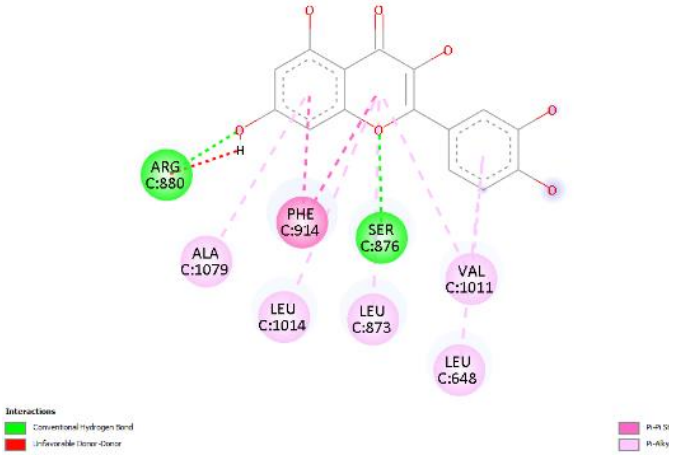	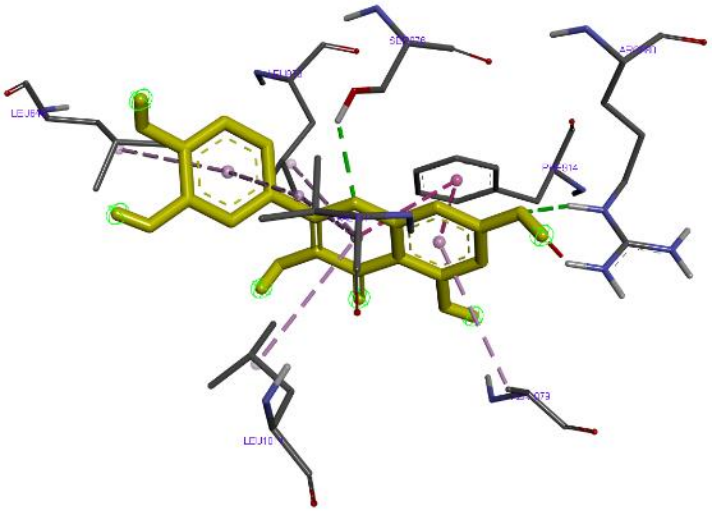
Myristicin	-5.6	Leu648, Asn768, Met770, Lys771, Glu802, Leu873, Val1011, Leu1014, Pro1076, Tyr1121	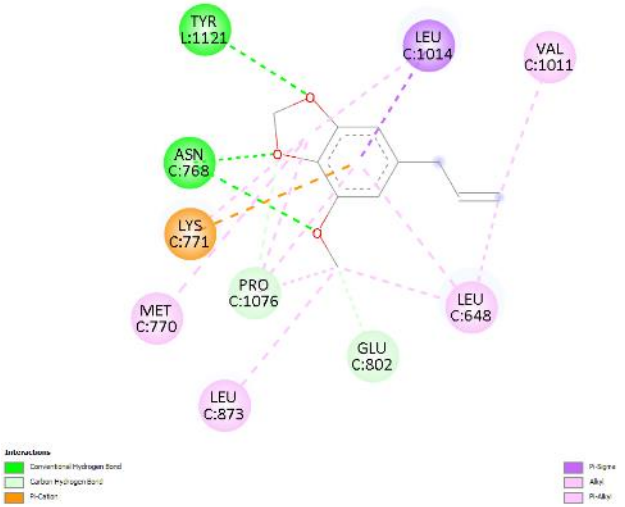	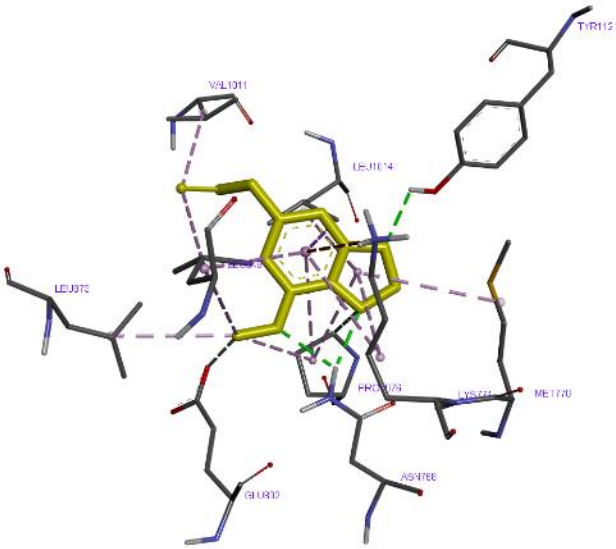

Stigmastane-hexol	-6.3	Lys771

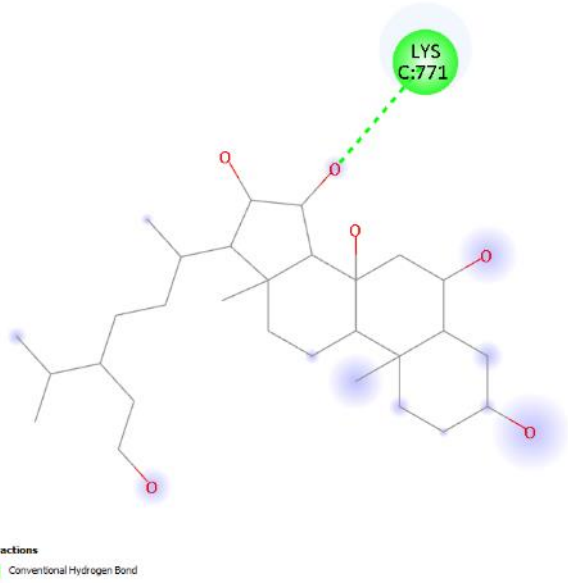

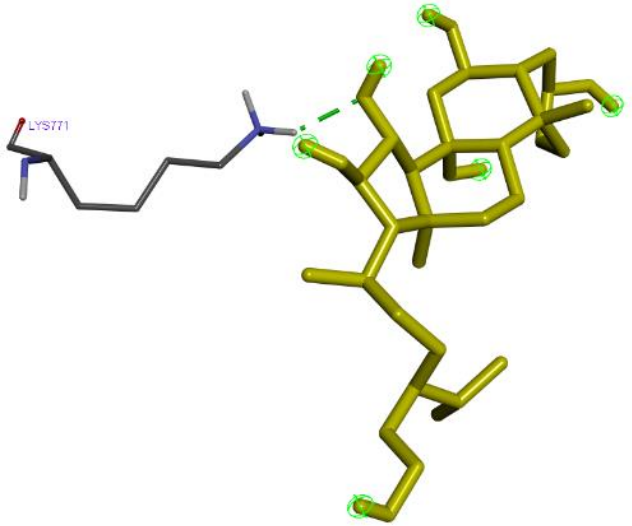

Reference (Febuxostat)	-8.4	Leu648, Phe649, Asn768, Glu802, Leu873, Arg880, Phe914, Phe1009, Thr1010, Val1011, Leu1014, Ala1079

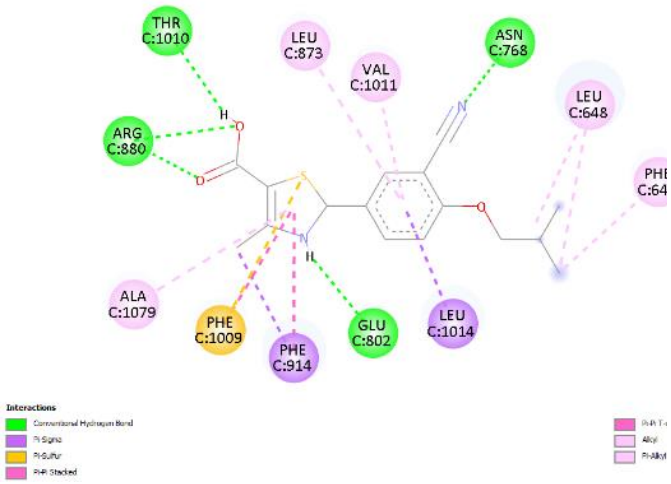

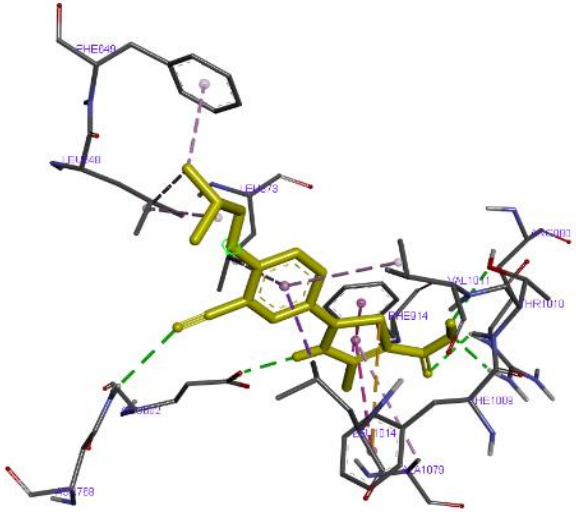

Antiproliferative (3ERT) RMSD : 1.400 Å				
Native ligand (4-Hydroxytamoxifen)	-9.5	Leu346, Ala350, Asp351, Glu353, Leu387, Met388, Met421, Leu525	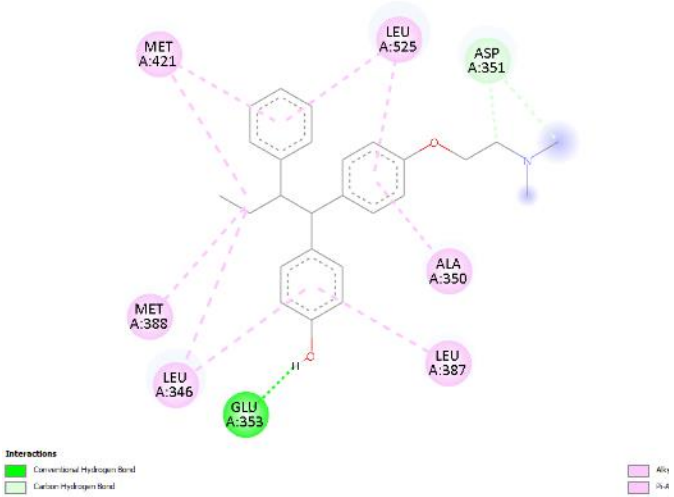	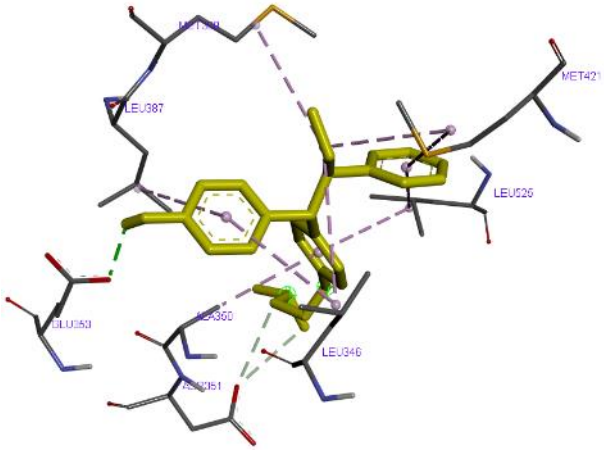
Myristicin	-6.2	Met343, Leu346, Ala350, Leu387, Leu391, Met421, Leu525	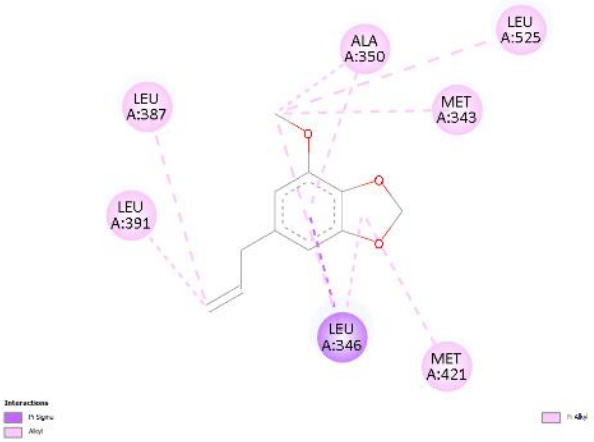	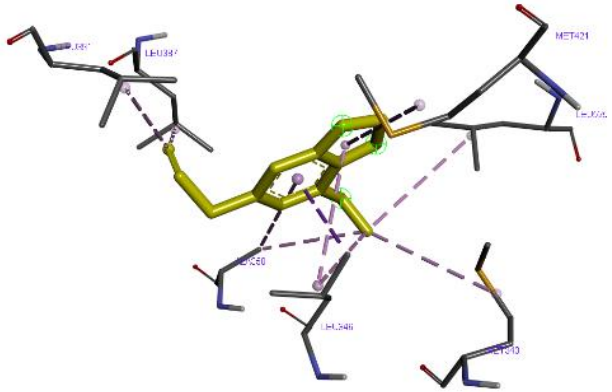

Quercetin	-7.9	Leu346, Ala350, Glu353, Leu387, Met388, Glu419, Gly420, Met421, Leu525	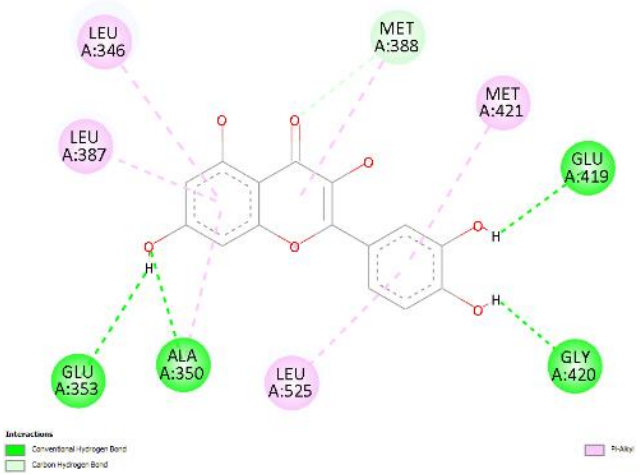	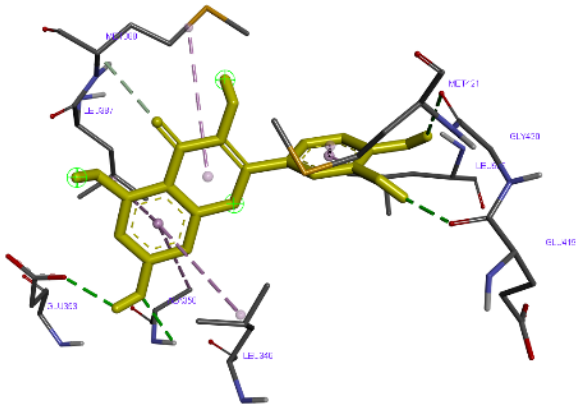
Stigmastane-hexol	-5.5	Met343, Leu346, Ala350, Trp383	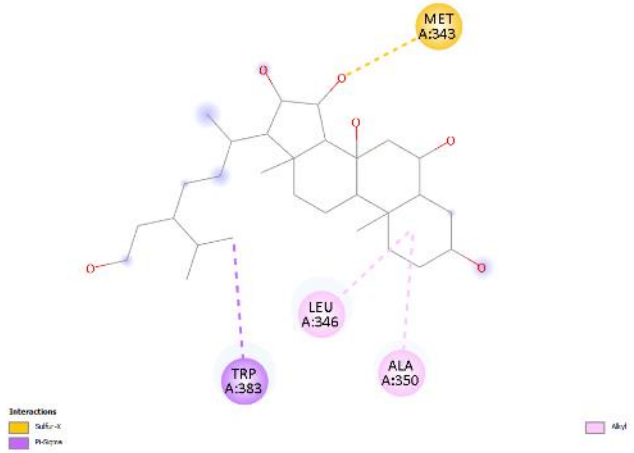	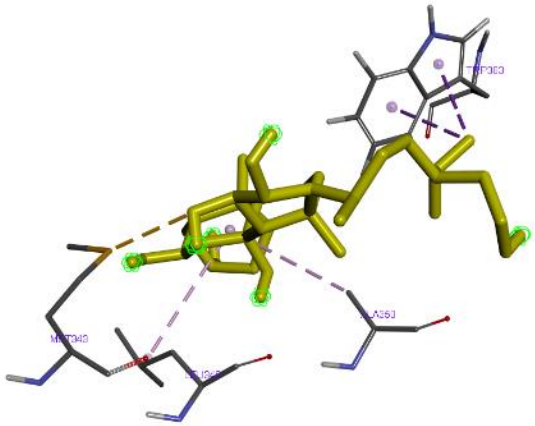

Antiproliferative 4JPS) RMSD : 0.700 Å				
Native ligand (Alpelisib)	-10.3	Ile800, Lys802, Ile848, Val850, Val851, Ser854, Gln859, Met922	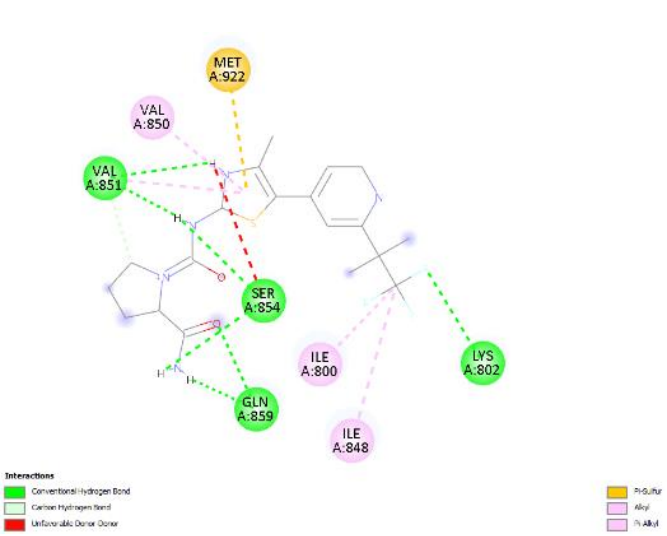	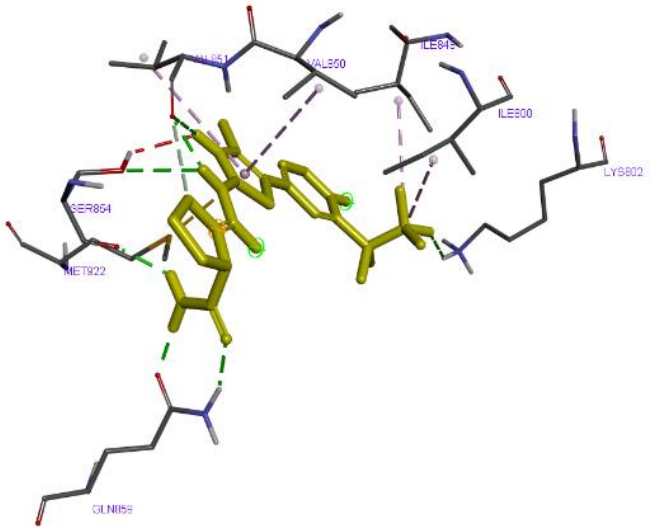
Myristicin	-6.4	Met772, Ile800, Tyr836, Ile848, Val851, Phe930, Ile932, Asp933	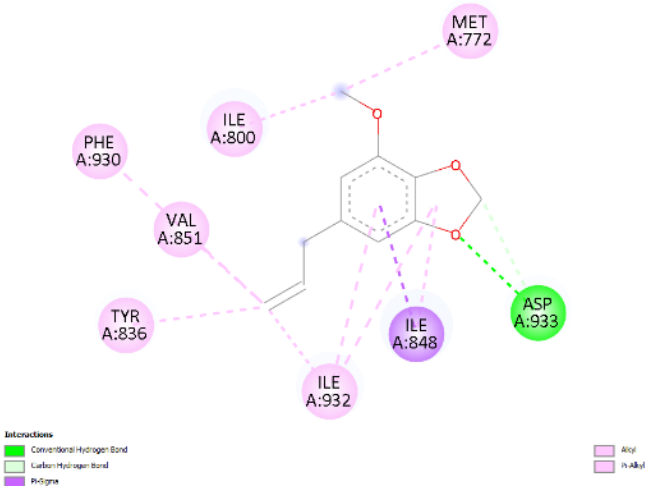	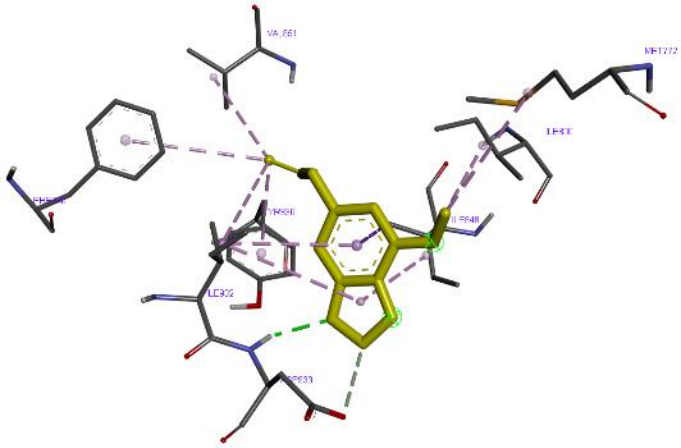

Quercetin	-8.4	Lys802, Tyr836, Ile848, Glu849, Val851, Met922, Ile932	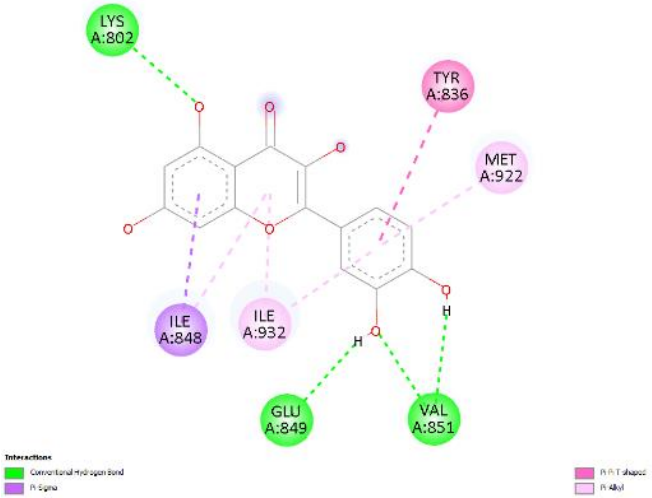	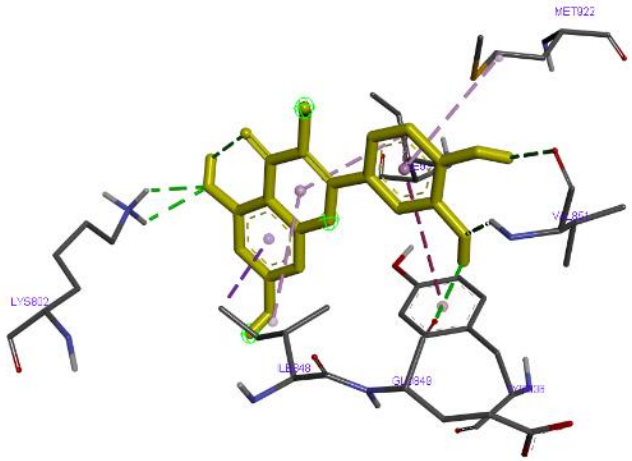
Stigmastane-hexol	-8.1	Glu821, Arg832, Pro835, Val850, Lys924	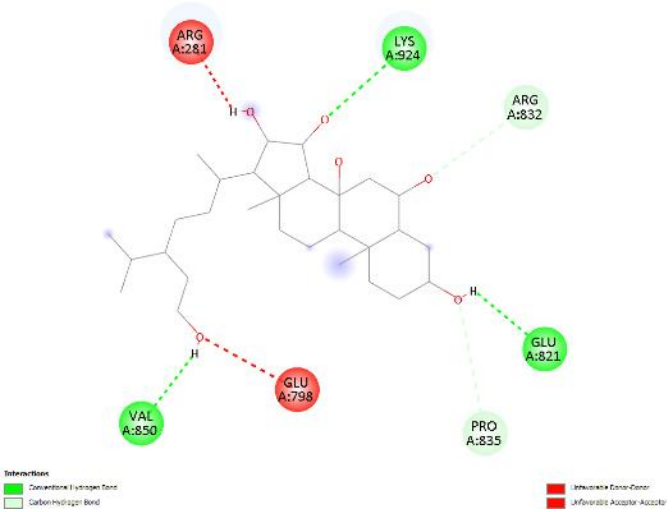	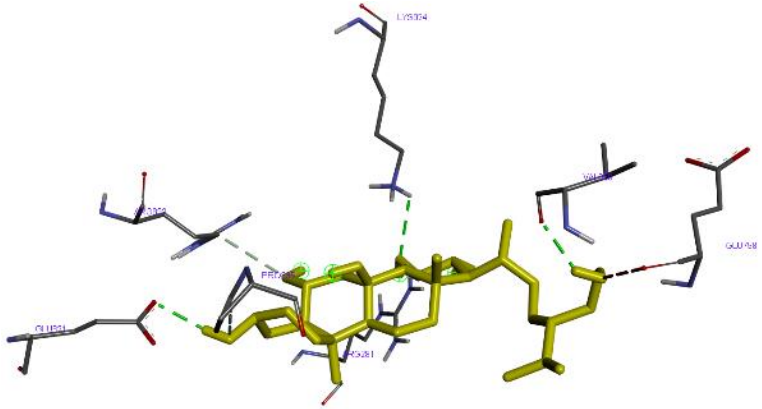

CONCLUSION

This study provides the first integrated correlation linking GC-MS, LC-HRMS, and docking with antioxidant and antiproliferative activities of *Myristica fragrans* leaf fractions. The ethyl acetate fraction, enriched in phenolics including quercetin, showed the strongest radical-scavenging capacity (IC_{50} 23.92 ± 2.75 µg/mL), while the hexane fraction, dominated by non-polar constituents, produced the lowest MCF-7 IC_{50} (131.125 µg/mL). Docking with redocking RMSD ≤ 2.0 Å supported quercetin as the most consistent binder across Keap1, XO, ERα, and PI3Kα, with stigmastane-hexol competitive in Keap1 and myristicin weaker, aligning with the fractional trends. Together, these data nominate ethyl acetate as an antioxidant source and hexane as a reservoir of membrane-active leads.

The novelty lies in coupling fraction-specific chemical space to orthogonal bioassays and benchmarking docking against reference ligands to rationalize the observed activities at the fraction level. Beyond *M. fragrans*, the workflow offers a general template for prioritizing semi-polar antioxidant fractions and non-polar cytotoxic fractions. Priority next steps include bioassay-guided isolation and absolute quantification of dominant actives, followed by mechanistic apoptosis studies in MCF-7 and comparator lines. Structure confirmation should integrate MS/MS and NMR with stereochemical assignment. To enhance translational relevance, assess selectivity against nonmalignant breast epithelial cells and extend to in vivo models with pharmacokinetics, tissue distribution, and basic safety endpoints.

ACKNOWLEDGEMENT

Appreciation is extended to the National Research and Innovation Agency (BRIN) for institutional support, with special thanks to the researchers at the Center for Research on Pharmaceutical Ingredients and Traditional Medicine, BRIN, for technical assistance and constructive input. Academic mentorship and scholarly feedback from the University of Indonesia are gratefully acknowledged for their contributions throughout the study.

REFERENCES

1. Lee, A. V., Oesterreich, S. and Davidson, N. E. (2015) MCF-7 cells: The first breast cancer cell line. *Journal of the National Cancer Institute*, **107(7)**, djv073.

2. Ashokkumar, K., Simal-Gandara, J., Murugan, M., Dhanya, M. K. and Pandian, A. (2022) Nutmeg (*Myristica fragrans* Houtt.) essential oil: A review on its composition, biological, and pharmacological activities. *Phytotherapy Research*, **36(7)**, 2839–2851.

3. Piaru, S. P., Mahmud, R., Abdul Majid, A. M., Ismail, S. and Man, C. N. (2012) Chemical composition, antioxidant and cytotoxicity activities of the essential oils of *Myristica fragrans* and *Morinda citrifolia*. *Journal of the Science of Food and Agriculture*, **92(3)**, 593–597.

4. Biswas, P., Dey, D., Biswas, P. K., Rahaman, T. I., Saha, S., Parvez, A., Khan, D. A., Lily, N. J., Saha, K., Sohel, M., Hasan, M. M., Al Azad, S., Bibi, S., Hasan, M. N., Rahmatullah, M., Chun, J., Rahman, M. A. and Kim, B. (2022) A comprehensive analysis and anti-cancer activities of quercetin in ROS-mediated cancer and cancer stem cells. *International Journal of Molecular Sciences*, **23(19)**, 11746.

5. Mohos, V., Panovics, A., Fliszar-Nyul, E., Schilli, G., Hetenyi, C., Mladenka, P., Needs, P. W., Kroon, P. A., Petho, G. & Poor, M. (2019) Inhibitory effects of quercetin and its human and microbial metabolites on xanthine oxidase enzyme. *International Journal of Molecular Sciences*, **20(11)**, 2681.

6. Cagliero, C., Bicchi, C., Marengo, A., Rubiolo, P. and Sgorbini, B. (2021) Gas chromatography of essential oil: state-of-the-art, recent advanced, and perspectives. *Journal Separation Science*, **45(1)**, 94–112.

7. Lopez-Fernandez, O., Domínguez, R., Pateiro, M., Munekata, P. E. S., Rocchetti, G. and Lorenzo, J. M. (2020) Determination of polyphenols using liquid chromatography-tandem mass spectrometry technique (LC-MS/MS): A review. *Antioxidants*, **9(6)**, 479.

8. Louw, S. (2021) Recent trends in the chromatographic analysis of volatile flavor and fragrance compounds: Annual review 2020. *Analytical Science Advances*, **2(3-4)**, 157–170.

9. Davies, T. G., Wixted, W. E., Coyle, J. E., Griffiths-Jones, C., Hearn, K., McMenamin, R., Norton, D., Rich, S. J., Richardson, C., Saxty, G., Willems, H. M. G., Woolford, A. J., Cottom, J. E., Kou, J. P., Yonchuk, J. G., Feldser, H. G., Sanchez, Y., Foley, J. P., Bolognese, B. J., Logan, G. and Kerns, J. K. (2016) Monoacidic inhibitors of the KEAP1:NRF2 protein-protein interaction with high cell potency identified by fragment-based discovery. *Journal of Medicinal Chemistry*, **59(8)**, 3991–4006.

10. Zhang, C., Wang, R., Zhang, G. and Gong, D. (2018) Mechanistic insights into the inhibition of quercetin on xanthine oxidase. *International Journal of Biological Macromolecules*, **112**, 405–412.

11. Shiau, A. K., Barstad, D., Loria, P. M., Cheng, L., Kushner, P. J., Agard, D. A. and Greene, G. L. (1998) The structural basis of estrogen receptor/ coactivator recognition and the antagonism of this interaction by tamoxifen. *Cell*, **95(7)**, 927–937.

12. Furet, P., Guagnano, V., Fairhurst, R. A., Imbach-Weese, P., Bruce, I., Knapp, M., Fritsch, C., Blasco, F., Blanz, J., Aichholz, R., Hamon, J., Fabbro, D. and Caravatti, G. (2013) Discovery of NVP-BYL719 a potent and selective phosphatidylinositol-3 kinase alpha inhibitor selected for clinical evaluation. *Bioorganic & Medicinal Chemistry Letters*, **23(13)**, 3741–3748.

13. Pagadala, N. S., Syed, K. and Tuszynski, J. (2017) Software for molecular docking and its validation criteria. *Current Topics in Medicinal Chemistry*, **17**, 1–16.

14. Crisman, E., Duarte, P., Dauden, E., Cuadrado, A., Rodriguez-Franco, M. I., Lopez, M. G. and Leon, R. (2023) KEAP1–NRF2 protein-protein interaction inhibitors: Design, pharmacological properties and therapeutic potential. *Medicinal Research Reviews*, **43**, 237–287.

15. RCSB Protein Data Bank (1998) *Estrogen receptor ligand-binding domain complexed with 4-hydroxytamoxifen* (PDB: 3ERT), RCSB Protein Data Bank.

16. RCSB Protein Data Bank (2014) *Crystal structure of p110α/p85α bound to BYL719 (alpelisib*) (PDB: 4JPS), RCSB Protein Data Bank.

17. Zhang, Q. W., Lin, L. G. and Ye, W. C. (2018) Techniques for extraction and isolation of natural products: A comprehensive review. *Chinese Medicine*, **13**, 20.

18. Shaikh, J. R. and Patil, M. K. (2020) Qualitative tests for preliminary phytochemical screening: An overview. *International Journal of Chemical Studies*, **8(2)**, 603–608.

19. Baky, M. H., El-Taher, E. M., Naggar, D. M. and Abouelela, M. (2024) Phytochemical investigation of the n-hexane-extracted oil from four umbelliferous vegetables using GC/MS analysis in the context of antibacterial activity. *Scientific Report*, **14**, 10592.

20. Nikolic, V., Nikolic, L., Dinic, A., Gajic, I., Urosevic, M., Stanojevic, L., Stanojevic, J. and Danilovic, B. (2021) Chemical composition, antioxidant and antimicrobial activity of nutmeg (*Myristica fragrans* Houtt.) seed essential oil. *Journal of Essential Oil-Bearing Plants*, **24(2)**, 218–227.

21. Khoerunisah, M. S., Angelina, M. and Kasiyati (2022) Cytotoxic test of *Cassia alata* L. leaves ethanol extracts, fractions, and main compounds against MCF-7 cells. *Indonesian Journal of Cancer Chemoprevention*, **13(3)**, 144–151.

22. Warren, G. L., Andrews, C. W., Capelli, A. M., Clarke, B., LaLonde, J., Lambert, M. H., Lindvall, M., Nevins, N., Semus, S. F., Senger, S., Tedesco, G., Wall, I. D., Woolven, J. M., Peishoff, C. E. and Head, M. S. (2006) A critical assessment of docking programs and scoring functions. *Journal of Medicinal Chemistry*, **49(20)**, 5912–5931.

23. Szewczyk, K., Dos-Santos, W., Pietrzak, K., Klimek, K., Grzywa-Celinska, A., Celinski, R. and Gogacz, M. (2022) LC-ESI-MS/MS identification of biologically active phenolics in different extracts of *Alchemilla acutiloba* Opiz. *Molecules*, **27**, 621.

24. El Sayed, A. M., Basam, S. M., El-Naggar, E. M. A., Marzouk, H. S. and El Hawary, S. (2020) LC-MS/MS and GC-MS profiling as well as the antimicrobial effect of leaves of selected Yucca species introduced to Egypt. *Scientific Reports*, **10**, 17778.

25. Zheng, Y., Sun, J., Luo, Z., Li, Y. and Huang, Y. (2024) Emerging mechanisms of lipid peroxidation in regulated cell death and its physiological implications. *Cell Death & Disease*, **15(11)**, 859.

26. Cuyckens, F. and Claeys, M. (2004) Mass spectrometry in the structural analysis of flavonoids. *Journal of Mass Spectrometry*, **39**, 1–15.

27. Li, Z. H., Guo, H., Xu, W. B., Ge, J., Li, X., Alimu, M. and He, D. J. (2016) Rapid identification of flavonoid constituents directly from PTP1B inhibitive extract of raspberry (*Rubus idaeus* L.) leaves by HPLC-ESI-QTOF-MS/MS. *Journal of Chromatographic Science*, **54(5)**, 805–810.

28. Veiko, A. G., Lapshina, E. A. and Zavodnik, I. B. (2021) Comparative analysis of molecular properties and reactions with oxidants for quercetin, catechin, and naringenin. *Molecular and Cellular Biochemistry*, **476**, 4287–4299.

29. Handayani, V., Ahmad, A. R. and Sudir, M. (2014) Uji aktivitas antioksidan ekstrak metanol bunga dan daun patikala (*Etlingera elatior* (Jack) R.M.Sm) menggunakan metode DPPH. *Pharmacy Science Research*, **1(2)**, 86–93.

30. Apak, R., Ozyurek, M., Guclu, K. and Capanoglu, E. (2016) Antioxidant activity/capacity measurement. 1. Classification, physicochemical principles, mechanisms, and electron transfer-based assays. *Journal of Agricultural and Food Chemistry*, **64(5)**, 997–1027.

31. Choi, S. S., Park, H. R. and Lee, K. A. (2021) A comparative study of rutin and rutin glycoside: Antioxidant activity, anti-inflammatory effect, effect on platelet aggregation and blood coagulation. *Antioxidants*, **10(11)**, 1696.

32. Nurmilasari, N., Ginting, B. and Helwati, H. (2017) Isolation of antioxidant compounds of methanol extract of nutmeg leaves (*Myristica fragrans* Houtt). *Journal Natural*, **17(1)**, 49–57.

33. Deghima, A., Righi, N., Rosales-Conrado, N., Leon-Gonzales, M. E., Baali, F., Gomez-Mejia, E., Madrid, Y. and Bedjou, F. (2021) Anti-inflammatory activity of ethyl acetate and n-butanol extracts from Ranunculus macrophyllus Desf. and their phenolic profile. *Journal of Ethnopharmacology*, **265**, 113347

34. Gvozdeva, Y. & Georgieva, P. (2025) therapeutic potential of essential oils and their bioactive compounds against colon cancer: focus on colon-specific micro- and nanocarriers. *BioChem*, **5(3)**, 26.

35. Adibuduge, Y. and Senevirathne, M. (2023) Potential of nutmeg (*Myristica fragrans* Houtt) leaf extracts as a source of functional ingredients with antibacterial, antifungal and antioxidant activities. *Journal of Agricultural Sciences (Sri Lanka)*, **18(2)**, 221–236.

36. Ginting, B., Hadijah, S. and Helwati, H. (2017) Isolation of antioxidant compounds of n-hexane extract of nutmeg (*Myristica fragrans* Houtt) leaves. *Jurnal Kimia Mulawarman*, **15(1)**, 46–52.

37. Anywar, G. U., Kakudidi, E., Oryem-Origa, H., Schubert, A. and Jassoy, C. (2022) Cytotoxicity of medicinal plant species used by traditional healers in treating people suffering from HIV/AIDS in Uganda. *Frontiers in Toxicology*, **4**, 832780.

38. Camara, J. S., Perestrelo, R., Ferreira, R., Berenguer, C. V., Pereira, J. A. M. and Castilho, P. C. (2024) Plant-derived terpenoids: A plethora of bioactive compounds with several health functions and industrial applications-A comprehensive overview. *Molecules*, **29(16)**, 3861.

39. Hu, L., Luo, Y., Yang, J. and Cheng, C. (2025) Botanical flavonoids: Efficacy, absorption, metabolism and advanced pharmaceutical technology for improving bioavailability. *Molecules*, **30(5)**, 1184.

40. Ginting, B., Nurdin, S., Murniana, Mustanir, Maulidna and Simanjuntak, P. (2020) Lignan compound isolated from n-hexane extract *Myristica fragrans* Houtt root as antioxidant and antitumor activities against MCF-7 cell lines data. *Data in Brief*, **31**, 105997.

41. Ginting, B., Mustanir, N., Maulidna, M., Murniana and Safrina (2021) Evaluation of antioxidant and anticancer activity of *Myristica fragrans* Houtt. Bark. *Pharmacognosy Journal*, **13(3)**, 780–786.

42. Poli, G., Martinelli, A. and Tuccinardi, T. (2016) Reliability analysis and optimization of the consensus docking approach for the development of virtual screening studies. *Journal of Enzyme Inhibition and Medicinal Chemistry*, **31(2)**, 167–173.

43. Shamsian, S., Sokouti, B. and Dastmalchi, S. (2024) Benchmarking different docking protocols for predicting the binding poses of ligands complexed with cyclooxygenase enzymes and screening chemical libraries. *BioImpacts*, **14(2)**, 29955.

44. Huang, Z., Peng, Z., Huang, D. and Zhou, Z. (2025) Virtual screening of KEAP1-NRF2 inhibitors and in vitro validation. *Molecules*, **30(8)**, 1815.

45. Davies, T. G., Wixted, W. E., Coyle, J. E., Griffiths-Jones, C., Hearn, K., McMenamin, R. L., Norton, D., Rich, S. J., Richardson, C., Saxty, G., Willems, H. M. G., Woolford, A. J., Cottom, J. E., Kou, J., Yonchuk, J. G., Feldser, H. G., Sanchez, Y., Foley, J. P., Bolognese, B. J. and Kerns, J. K. (2016) *Structure of the Keap1 Kelch domain in complex with a small molecule inhibitor* (PDB ID: 5FNU), RCSB Protein Data Bank.

46. Rocha-Roa, C., Cortes, E., Cuesta, S. A., Mora, J. R., Paz, J. L., Flores-Sumoza, M. and Márquez, E. A. (2023) Study of potential inhibition of the estrogen receptor α by cannabinoids using an in silico approach: Agonist vs antagonist mechanism. *Computers in Biology and Medicine*, **152**, 106403.

47. Alamri, A., Rauf, A., Khalil, A. A., Alghamdi, A., Alafnan, A., Alshammari, A., Alshammari, F., Malik, J. A. and Anwar, S. (2021) In silico

screening of marine compounds as an emerging and promising approach against estrogen receptor alpha-positive breast cancer. *BioMed Research International*, **2021**, 9734279.

48. Zhang, M., Jang, H. and Nussinov, R. (2020) PI3K inhibitors: Review and new strategies. *Chemical Science*, **11**, 5855–5865.

49. Culletta, G., Buttari, B., Arese, M., Brogi, S., Almerico, A. M., Saso, L. and Tutone, M. (2024) Natural products as non-covalent and covalent modulators of the KEAP1/NRF2 pathway exerting antioxidant effects. *European Journal of Medicinal Chemistry*, **270**, 116355.

50. Olla, S., Siguri, C., Fais, A., Era, B., Fantini, M. C. and Di Petrillo, A. (2023) Inhibitory effect of quercetin on oxidative endogen enzymes: A focus on putative binding modes. *International Journal of Molecular Sciences*, **24(20)**, 15391.